Cell Reports

Article

Protein disulfide isomerase PDI-6 regulates Wnt secretion to coordinate inter-tissue UPR^{mt} activation and lifespan extension in *C. elegans*

Graphical abstract

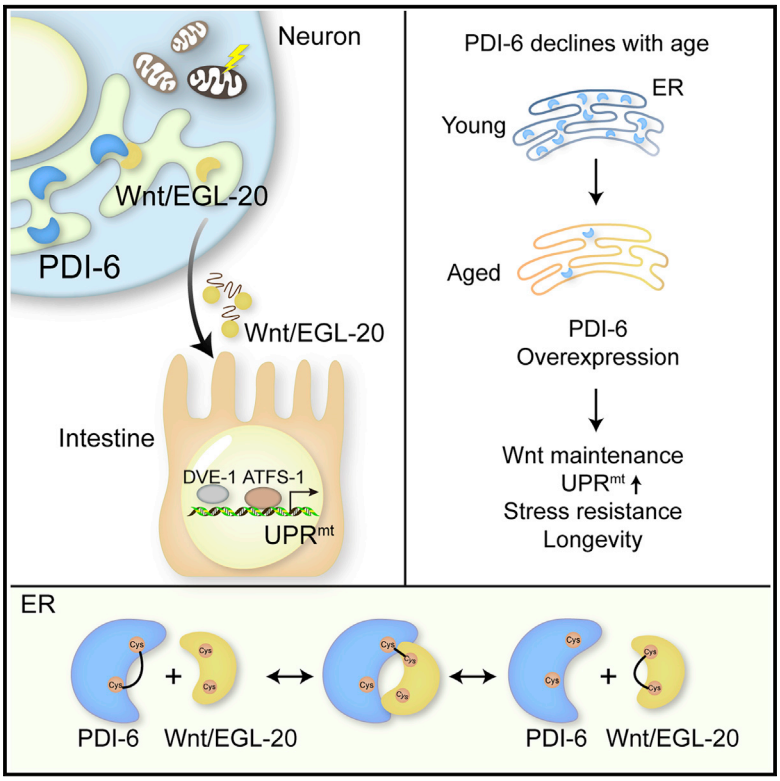

Highlights

- *pdi-6* deficiency suppresses the cell-non-autonomous UPR^{mt} signaling
- PDI-6 mediates Wnt/EGL-20 secretion to coordinate inter-tissue UPR^{mt} signaling
- PDI-6 interacts with EGL-20 via disulfide bonds
- Overexpression of PDI-6 confers on animals stress resistance and longevity

Authors

Xinyu Li, Jiasheng Li, Di Zhu, ..., Yangli Liu, Xueying Wu, Ye Tian

Correspondence

ytian@genetics.ac.cn

In brief

Li et al. show that the protein disulfide isomerase PDI-6 interacts with Wnt/EGL-20 in the endoplasmic reticulum to regulate Wnt/EGL-20 stability and secretion for cell-non-autonomous UPR^{mt} activation and lifespan regulation.

Li et al., 2022, Cell Reports *39*, 110931
June 7, 2022
https://doi.org/10.1016/j.celrep.2022.110931

CellPress

Cell Reports

CellPress
OPEN ACCESS

Article

Protein disulfide isomerase PDI-6 regulates Wnt secretion to coordinate inter-tissue UPR^{mt} activation and lifespan extension in *C. elegans*

Xinyu Li,[1,2] Jiasheng Li,[1,2] Di Zhu,[1,2] Ning Zhang,[1,2] Xusheng Hao,[1,2] Wenfeng Zhang,[1,2] Qian Zhang,[1] Yangli Liu,[1] Xueying Wu,[1] and Ye Tian[1,2,3,4,*]

[1]State Key Laboratory of Molecular Developmental Biology, Institute of Genetics and Developmental Biology, Chinese Academy of Sciences, Beijing 100101, China

[2]University of Chinese Academy of Sciences, Beijing 100093, China

[3]Center for Excellence in Animal Evolution and Genetics, Chinese Academy of Sciences, Kunming 650223, China

[4]Lead contact

*Correspondence: ytian@genetics.ac.cn

https://doi.org/10.1016/j.celrep.2022.110931

SUMMARY

Coordination of inter-tissue stress signaling is essential for organismal fitness. Neuronal mitochondrial perturbations activate the mitochondrial unfolded-protein response (UPR^{mt}) in the intestine via the mitokine Wnt signaling in *Caenorhabditis elegans*. Here, we found that the protein disulfide isomerase PDI-6 coordinates inter-tissue UPR^{mt} signaling via regulating the Wnt ligand EGL-20. PDI-6 is expressed in the endoplasmic reticulum (ER) and interacts with EGL-20 through disulfide bonds that are essential for EGL-20 stability and secretion. *pdi-6* deficiency results in misfolded EGL-20, which leads to its degradation via ER-associated protein degradation (ERAD) machinery. Expression of PDI-6 declines drastically with aging, and animals with *pdi-6* deficiency have decreased lifespan. Overexpression of PDI-6 is sufficient to maintain Wnt/EGL-20 protein levels during aging, activating the UPR^{mt}, and significantly extending lifespan in a Wnt- and UPR^{mt}-dependent manner. Our study reveals that protein disulfide isomerase facilitates Wnt secretion to coordinate the inter-tissue UPR^{mt} signaling and organismal aging.

INTRODUCTION

Multicellular organisms must coordinate stress responses across different tissues to maintain organismal homeostasis in the face of an ever-changing environment (Frakes and Dillin, 2017; Taylor and Dillin, 2013; Zhang et al., 2018b). Inter-tissue communication of mitochondrial stress signals has been reported in humans and multiple model organisms. For example, human patients with mitochondrial diseases, such as infantile-onset spinocerebellar ataxia (IOSCA), show muscle debilitation and produce excess levels of FGF21, a cytokine that enters and circulates in the blood (Suomalainen et al., 2011). *Drosophila melanogaster* with disrupted muscle mitochondrial function have elevated levels of ImpL2 (an ortholog to human insulin-like growth factor-binding protein 7), which systemically antagonizes insulin signaling and prolongs lifespan (Owusu-Ansah et al., 2013). Mild mitoribosomal stress in mouse pro-opiomelanocortin (POMC) neurons leads to a high metabolic turnover, activating thermogenesis and the mitochondrial unfolded-protein response (UPR^{mt}) in adipose tissues (Kang et al., 2021).

The UPR^{mt} is a mitochondrial stress response that transcriptionally increases the expression of mitochondrial quality control genes to restore mitochondrial proteostasis (Shpilka and Haynes, 2018). Although severe loss of mitochondrial function is detrimental, some studies have shown that partial suppression of the mitochondrial activity activates the UPR^{mt} and promotes longevity in multiple model organisms (Copeland et al., 2009; Dillin et al., 2002; Durieux et al., 2011; Feng et al., 2001; Liu et al., 2005). Activation of the UPR^{mt} requires the transcription factor ATFS-1, the chromatin modifier DVE-1, and multiple histone-modifying enzymes such as histone methyltransferase MET-2/LIN-65, histone demethylases JMJDs, and histone deacetylation NuRD complex (Haynes et al., 2010; Li et al., 2021; Merkwirth et al., 2016; Nargund et al., 2012; Shao et al., 2020; Tian et al., 2016; Zhu et al., 2020, 2022).

Several inter-tissue communications of mitochondrial stress signaling have been demonstrated in *Caenorhabditis elegans*. For example, knockdown of the mitochondrial electron transport chain (ETC) subunits, specifically in the nervous system, activates UPR^{mt} in the intestine and extends lifespan (Durieux et al., 2011; Shao et al., 2016). Furthermore, expression of the Huntington's disease-causing polyglutamine expansion protein (Q40) in neurons results in the induction of UPR^{mt} in peripheral tissues (Berendzen et al., 2016; Brignull et al., 2006; Morley et al., 2002; Zhang et al., 2018b). Perturbation of neuronal mitochondrial dynamics induces cell-non-autonomous UPR^{mt} and controls global mitochondrial state (Chen et al., 2021). The cell-non-autonomous activation of UPR^{mt} requires the active

participation of the neurotransmitter serotonin; however, serotonin alone is not sufficient to induce the UPR^{mt} (Berendzen et al., 2016). Thus, it was hypothesized that the UPR^{mt} signal can be transmitted across multiple tissues via the action of secreted signals, termed mitokines, that are produced by the cells experiencing mitochondrial stress, propagated, and perceived by peripheral cells to activate the UPR^{mt} in distal tissues, and preparing the entire organism to respond to locally sensed mitochondrial stresses (Berendzen et al., 2016; Durieux et al., 2011; Zhang et al., 2018b). However, the nature and action of mitokine signals have remained largely elusive.

Our previous study found that Wnt/EGL-20 is a mitokine signal not only required but also sufficient to propagate UPR^{mt} signaling from neurons to peripheral tissues (Berendzen et al., 2016; Zhang and Tian, 2022; Zhang et al., 2018b, 2021). Furthermore, neuronally overexpressed Wnt ligand EGL-20 is sufficient to activate cell-non-autonomous UPR^{mt} in a retromer complex- and serotonin-dependent manner and induces lifespan extension in *C. elegans* (Zhang et al., 2018b). Wnt is a secreted signal typically associated with cell polarity establishment, cell proliferation, and cell fate decision processes during development (Arata et al., 2006; Goldstein et al., 2006; Mizumoto and Sawa, 2007; Nusse and Clevers, 2017; Sugioka et al., 2011). However, little is known about how the Wnt protein perceives mitochondrial stress stimuli and acts as a signal molecule to coordinate UPR^{mt} signaling across multiple tissues.

Here, we performed an ethyl methanesulfonate (EMS) screen to identify genes required for cell-non-autonomous activation of UPR^{mt} in *C. elegans*, utilizing the established system in which Wnt/EGL-20 overexpression in the nervous system elicits UPR^{mt} in the intestine. We characterized mutants that are defective in cell-non-autonomous UPR^{mt} signaling but retain the ability to induce cell-autonomous UPR^{mt}. We determined that PDI-6, a protein disulfide isomerase (PDI) in the endoplasmic reticulum (ER), is required for inter-tissue communication of UPR^{mt} signaling via its action in Wnt/EGL-20-producing cells. We further show that PDI-6 interacts with Wnt/EGL-20 potentially via intermolecular disulfide bonds, which are essential for Wnt/EGL-20 stability and activity. Loss of functional PDI-6 is shown to shorten lifespan, and overexpression of PDI-6 is sufficient to maintain Wnt/EGL-20 protein levels during aging, activate UPR^{mt} in the intestine, and promote longevity. In summary, our study reveals that PDI-6 mediates the cell-non-autonomous UPR^{mt} communication and lifespan through regulating the mitokine Wnt signal.

RESULTS

PDI-6 is required for cell-non-autonomous UPR^{mt} signaling

Neuronal overexpression of a Wnt ligand, EGL-20, is sufficient to induce the UPR^{mt} in the *C. elegans* intestine (Zhang et al., 2018b). UPR^{mt} activation can be monitored by assessing nuclear redistribution of the translational reporter DVE-1::GFP, which is a transcription factor (TF) essential for the UPR^{mt} (Haynes et al., 2007). We performed an EMS mutagenesis screen using the DVE-1::GFP reporter to identify mutants that suppress UPR^{mt} in the peripheral tissue of animals overexpressing neuronal Wnt/EGL-20 under the control of the *rgef-1* promoter, the cell-non-autonomous UPR^{mt} model that we established in our previous study (Zhang et al., 2018b). Subsequently, we evaluated whether the mutants identified in this screen retained their ability to activate UPR^{mt} in the intestine in response to cell-autonomous mitochondrial stress, such as *cco-1* RNAi delivered by bacterial feeding (Durieux et al., 2011). We have screened approximately 3,400 mutagenized genomes and got 42 mutants. Among these mutants, we have identified mutations in *mig-14(yth56)*, which encodes the secretion receptor of Wnt protein, and *lin-40(yth27)*, which encodes the scaffold protein of the nucleosome remodeling and histone deacetylase (NuRD) complex (Zhu et al., 2020). In this study, we focused on the mutant *yth16*, because of the strong suppression phenotype of the cell-non-autonomous UPR^{mt} (Figure 1A).

Single-nucleotide polymorphism (SNP) mapping and whole-genome deep sequencing indicated that *yth16* carries a mutation in *pdi-6* at the codon for amino acid 206, causing an alanine changed to a threonine. And expression of *pdi-6* rescued the suppressed *dve-1p*::*dve-1*::*gfp* phenotype in *pdi-6(yth16)* mutants (Figures 1A and 1B). *pdi-6* encodes a conserved PDI that is responsible for disulfide bond formation, breakage, or rearrangement of proteins in the ER (Feige and Hendershot, 2011). An additional point mutation in the *bar-1* splice site, which sits very close to *pdi-6* in the genetic map, was identified in *yth16*. BAR-1 is a β-catenin homolog, which interacts with the transcription factor POP-1/TCF to activate the canonical Wnt signaling pathway (Nusse and Clevers, 2017). To rule out any effect of the *bar-1* mutation, we generated several *pdi-6* deletion mutants by CRISPR-Cas9 editing. *pdi-6* is an essential gene; a homozygous strain (*ok1373*) retaining only the N-terminal 200 amino acids of PDI-6 is larval lethal (Eletto et al., 2014). We therefore generated several partial-loss-of-function alleles by deleting part of the two catalytic thioredoxin-like domains (a and a′) of PDI-6 (Figure S1A). Among these mutants, *pdi-6(yth104)* and *pdi-6(yth109)* contained a 162-bp and a 195-bp deletion, respectively, including the sequence encoding the first CGHC redox-active site. *pdi-6(yth112)* contained a 24-bp deletion before the sequence encoding the second CGHC redox-active site (Figure S1A). The other mutant alleles of *pdi-6* containing deletions in the sequence encoding the second CGHC redox-active site are larval lethal (Figure S1A), suggesting that the second CGHC motif of PDI-6 is indispensable for *C. elegans* development.

To investigate whether *pdi-6* is required for cell-non-autonomous UPR^{mt} signaling, we examined the UPR^{mt} induction in the intestine of different *pdi-6* mutant alleles that we obtained in animals overexpressing neuronal Wnt/EGL-20. *hsp-6* encodes a mitochondrial localized *hsp70* heat shock protein family member and is transcriptionally upregulated by UPR^{mt} activation (Yoneda et al., 2004). *yth104*, *yth109*, and *yth112* all significantly suppressed the induction of *hsp-6p*::*gfp* expression in the intestine in animals with neuronal Wnt/EGL-20 overexpression (Figures S1B and S1C). *yth112* was selected for further experiments because it showed the strongest suppression of the cell-non-autonomous UPR^{mt} phenotype. Various mitochondrial stresses in neurons can activate the cell-non-autonomous UPR^{mt}. For instance, expression of a polyglutamine repeat

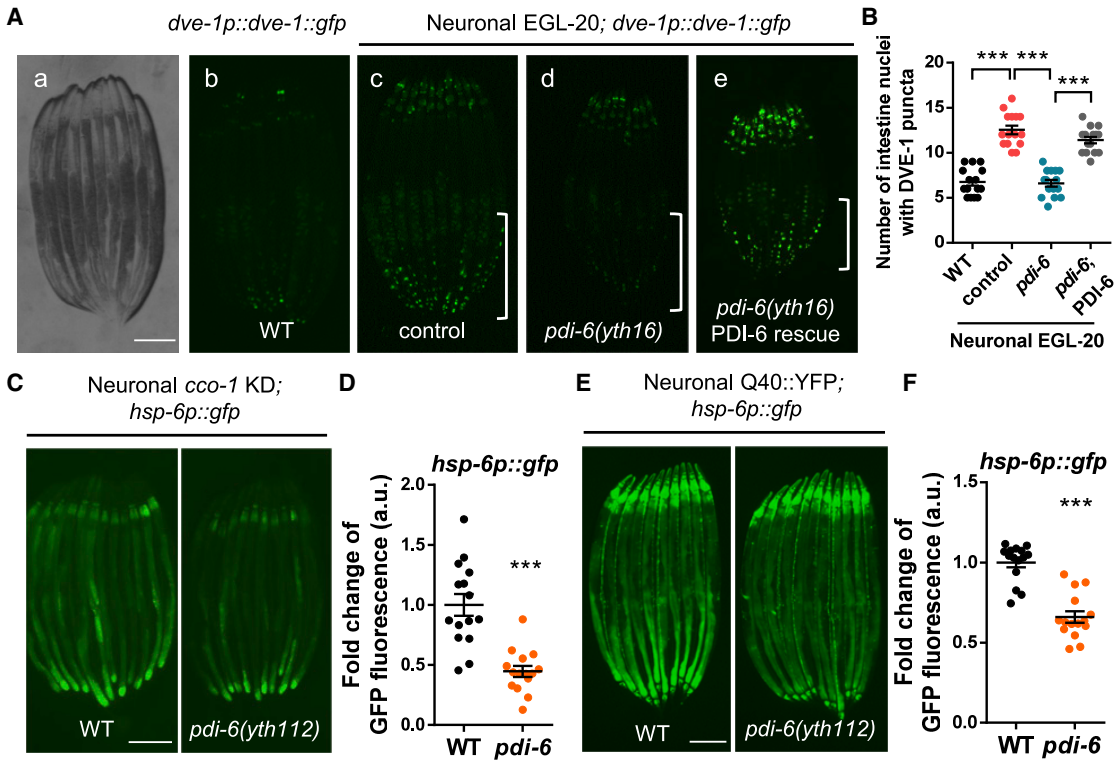

Figure 1. PDI-6 is required for cell-non-autonomous UPR^{mt} signaling

(A) Representative photomicrographs showing bright-field images of aligned, wild-type (WT) animals (a); *dve-1p*::*dve-1*::*gfp* expression in WT animals (b); *dve-1p*::*dve-1*::*gfp* upregulation in the intestine of day 2 adult animals expressing *rgef-1p*::*egl-20* (c); suppressed induction of *dve-1p*::*dve-1*::*gfp* in *pdi-6(yth16)* mutants (d); and *pdi-6(yth16)* mutants with *pdi-6p*::*pdi-6*::*mCherry* expression (e). The posterior region of the intestine where *dve-1p*::*dve-1*::*gfp* is induced or suppressed is highlighted in (c), (d), and (e).

(B) Quantification of intestinal nuclei with *dve-1p*::*dve-1*::*gfp* puncta in wild-type (WT) animals (b) and animals expressing *rgef-1p*::*egl-20* with the presence (c) or absence of the *pdi-6* mutation (d) and PDI-6 rescue (e), as shown in (A).

(C) Representative photomicrographs of day 1 adult animals with neuron-specific *cco-1* knockdown (KD) *unc-119p*::*cco-1* hairpin (HP), *sid-1(qt9)*, and *hsp-6p*::*gfp* in WT and *pdi-6* mutant animals.

(D) Quantification of *hsp-6p*::*gfp* expression as shown in (C).

(E) Representative photomicrographs of day 1 adult animals expressing *rgef-1p*::*Q40*::*yfp* and *hsp-6p*::*gfp* in WT and *pdi-6* mutant animals.

(F) Quantification of the *hsp-6p*::*gfp* expression as shown in (E).

***$p < 0.001$ (t test). Error bars, SEM. $n \geq 15$ worms. Scale bar, 250 μm.

See also Figure S1.

protein of 40 repeats (Q40) or knockdown (KD) of the mitochondrial ETC subunit *cco-1* in neurons activates UPR^{mt} in the peripheral tissue (Berendzen et al., 2016; Durieux et al., 2011). *pdi-6(yth112)* mutants also significantly suppressed *hsp-6p*::*gfp* expression in animals with neuronal *cco-1* KD or neuronal Q40::YFP expression (Figures 1C–1F). Furthermore, the induction of intestinal UPR^{mt} in *pdi-6* mutant animals was not affected when animals were treated with the cell-autonomous stressor *cco-1* RNAi via bacterial feeding (Figures S1D and S1E). We thus concluded that *pdi-6* is required for cell-non-autonomous UPR^{mt} signaling.

The ER unfolded-protein response (UPR^{ER}) and cytosolic unfolded-protein response (UPR^{cyt}) can also function in a cell-non-autonomous manner to coordinate stress response across multiple tissues (Douglas et al., 2015; Taylor and Dillin, 2013). *hsp-4* encodes the *C. elegans* ortholog of the ER chaperone BiP and is transcriptionally upregulated by UPR^{ER} (Calfon et al., 2002). The neuronal-expressing XBP-1 spliced form, the TF of UPR^{ER}, is sufficient to activate UPR^{ER} in the intestine (Taylor and Dillin, 2013). *hsp-16.2* encodes a small hsp20/alpha-B crystalline family member and is transcriptionally responsive to UPR^{cyt} mediated by the TF HSF-1 (Link et al., 1999). Neuronal HSF-1 independently regulates thermotolerance and longevity. The longevity is regulated by neuronal HSF-1 signaling to intestinal DAF-16, and *sod-3* is a canonical target of DAF-16 (Douglas et al., 2015). We therefore further examined the involvement of *pdi-6* in the cell-non-autonomous UPR^{ER} and oxidative-stress responses. Our results showed that *pdi-6* was not required for the cell-non-autonomous induction of UPR^{ER} or oxidative-stress response (Figures S1F–S1I). We found that UPR^{ER} was further enhanced in *pdi-6* mutants in response to RNAi for *ero-1*, which encodes the endoplasmic reticulum oxidase, whereas UPR^{cyt} was comparable between *pdi-6* mutants and wild-type animals treated by heat shock (Figures S1J–S1M). *pdi-6* deficiency

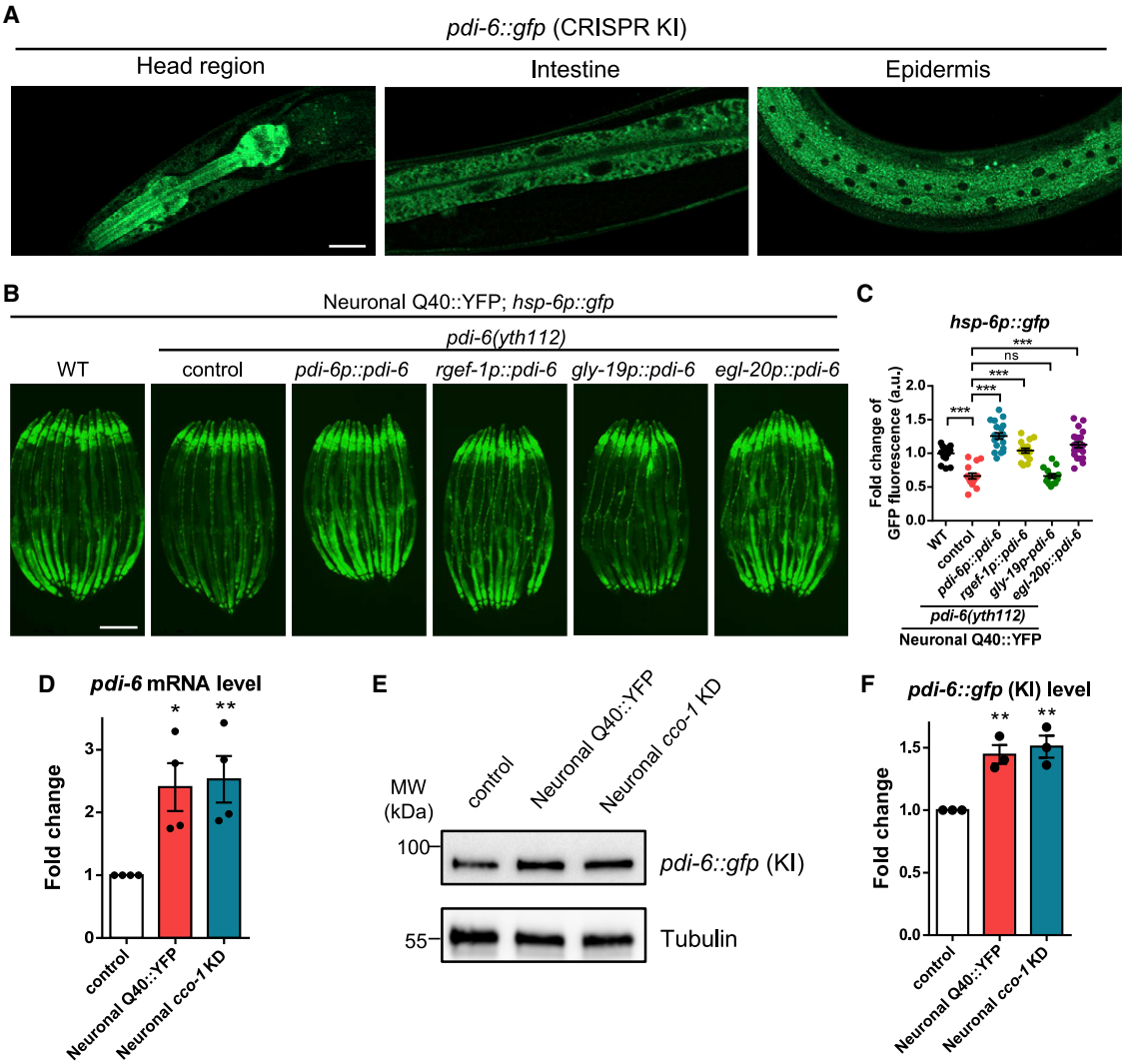

Figure 2. PDI-6 acts in Wnt/EGL-20-producing cells to mediate cell-non-autonomous UPR^{mt} activation

(A) Representative confocal photomicrographs of the head region, epidermis, and intestine in L4 animals expressing *pdi-6*::*gfp* (CRISPR-mediated GFP knockin). Scale bar, 20 μm.

(B) Representative photomicrographs of *rgef-1p*::*Q40*::*yfp*; *hsp-6p*::*gfp*, WT, and *pdi-6(yth112)* day 1 adult animals with or without *pdi-6p*::*pdi-6*::*mCherry*, *rgef-1p*::*pdi-6*, *gly-19p*::*pdi-6*, or *egl-20p*::*pdi-6* expression as indicated. Scale bar, 250 μm.

(C) Quantification of *hsp-6p*::*gfp* expression as shown in (B); n ≥ 15 worms.

(D) Quantification of *pdi-6* mRNA levels in young adult WT, *rgef-1p*::*Q40*::*yfp*, and *unc-119p*::*cco-1* HP; *sid-1(qt9)* animals. *p < 0.05, **p < 0.01 (t test). Error bars, SEM; n ≥ 3.

(E) Immunoblot of young adult *pdi-6*::*gfp* (CRISPR-mediated GFP knockin) expression in WT, *rgef-1p*::*Q40*::*YFP*, and *unc-119p*::*cco-1* HP; *sid-1(qt9)* animals.

(F) Quantification of *pdi-6*::*gfp* protein level as shown in (E); n ≥ 3.

*p < 0.05; **p < 0.01; ***p < 0.001; ns, not significant (p > 0.05, t test). Error bars, SEM.

See also Figure S2.

thus appears to sensitize animals to ER stress cell-autonomously but does not affect UPR^{cyt}.

PDI-6 acts in Wnt/EGL-20-producing cells to mediate cell-non-autonomous UPR^{mt} signaling

To identify which tissue is essential for PDI-6 in the regulation of cell-non-autonomous UPR^{mt} activation, we performed rescue experiments to induce *pdi-6* expression by using tissue-specific promoters in *pdi-6(yth112)* mutants with neuronal Q40::YFP expression. The expression pattern of PDI-6 was examined using animals with CRISPR-Cas9-mediated GFP knockin at the locus of endogenous *pdi-6* C terminus (*pdi-6*::*gfp*). PDI-6 was ubiquitously expressed in the epidermis, the intestine, and the head region (Figure 2A). We found that the expression of *pdi-6* with its native promoter strongly rescued the suppression of *hsp-6p*::*gfp* signals in the intestine of *pdi-6(yth112)* mutant

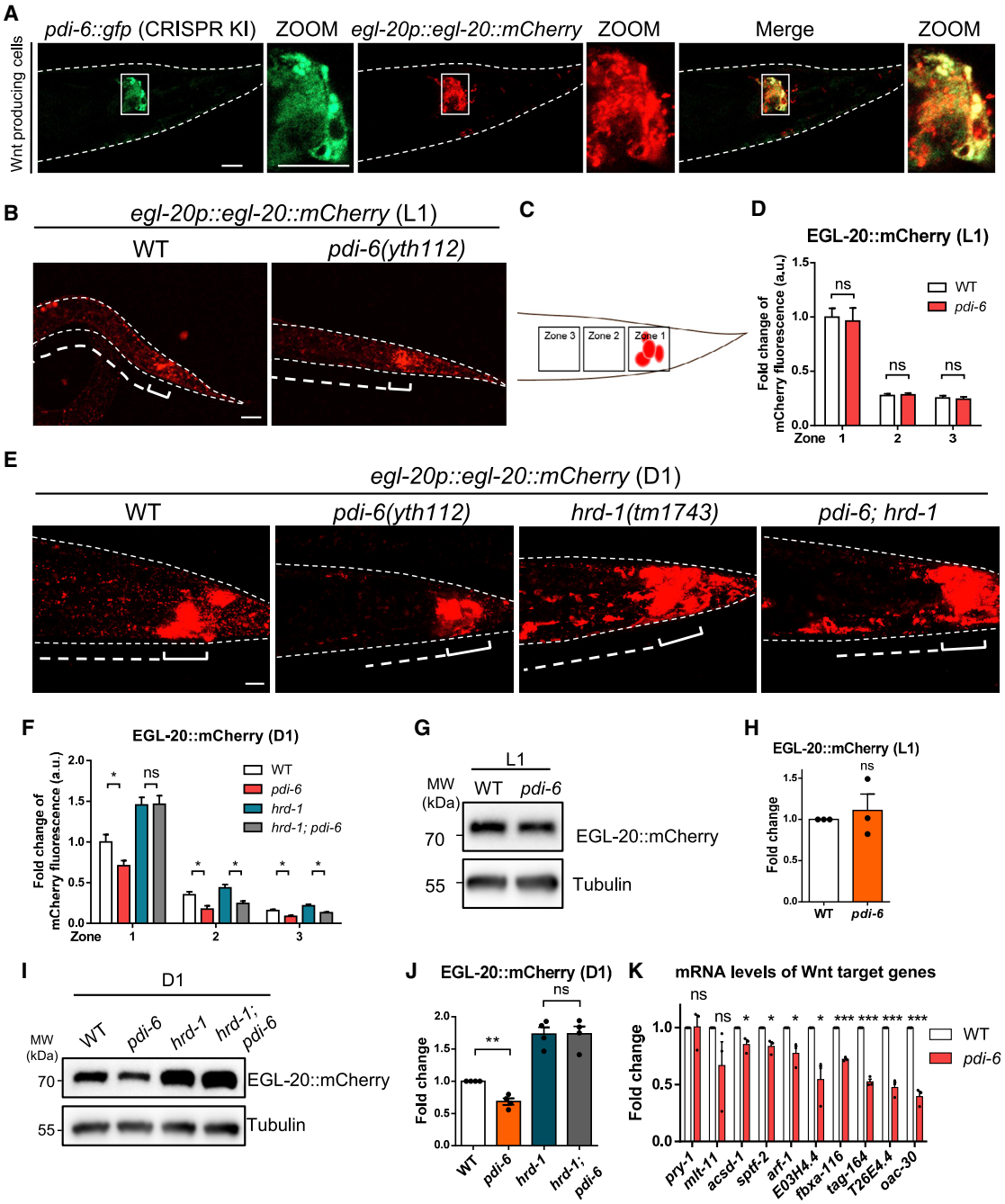

Figure 3. PDI-6 is required for Wnt/ELG-20 stability and gradient formation at adult stage

(A) Representative confocal photomicrographs of day 1 adult animals with *pdi-6*::*gfp* (CRISPR-mediated GFP knockin) in combination with *egl-20p*::*egl-20*::*mCherry*. Side panels show high-magnification views of boxed regions.

(B) Representative confocal photomicrographs of *egl-20p*::*egl-20*::*mCherry* at larval L1 stage of WT and *pdi-6(yth112)* mutant animals.

(C) Schematic of the posterior part of an animal expressing *egl-20p*::*egl-20*::*mCherry* from a group of posterior cells (red circles). EGL-20::mCherry levels measured in zones 1–3.

(D) Fold change of EGL-20::mCherry fluorescence of WT and *pdi-6* mutant animals in each zone of L1 larval stage.

(E) Representative confocal photomicrographs of *egl-20p*::*egl-20*::*mCherry* at day 1 (D1) of the adult stage of WT, *pdi-6(yth112)*, *hrd-1(tm1743)*, and *pdi-6(yth112)*; *hrd-1(tm1743)* mutant animals.

(F) Fold change of EGL-20::mCherry fluorescence of WT, *pdi-6*, *hrd-1* and *pdi-6*; *hrd-1* mutant animals in each zone of D1 adult stage.

(G) Immunoblot of *egl-20p*::*egl-20*::*mCherry* expression in L1 animals as indicated.

(H) Quantification of *egl-20p*::*egl-20*::*mCherry* levels as shown in (G).

(legend continued on next page)

animals with neuronal Q40::YFP expression (Figures 2B and 2C). However, the expression of *pdi-6* under the control of the intestinal *gly-19* promoter failed to restore cell-non-autonomous UPR^{mt} signaling in the *pdi-6(yth112)* mutants (Figures 2B and 2C). Furthermore, expression of *pdi-6* with the pan-neuron *rgef-1* promoter strongly rescued the suppression of cell-non-autonomous UPR^{mt} in the *pdi-6(yth112)* mutants (Figures 2B and 2C). Next, since Wnt/EGL-20 is required in the cell-non-autonomous UPR^{mt} regulation (Zhang et al., 2018b), we examined whether PDI-6 acts in Wnt/EGL-20-producing cells. Intriguingly, expressing *pdi-6* specifically in the Wnt/EGL-20 producing cells with *egl-20* promoter also strongly rescued the cell-non-autonomous UPR^{mt} activation in the *pdi-6(yth112)* mutants (Figures 2B and 2C). Additionally, the endogenous *pdi-6* mRNA levels were significantly increased in animals with neuronal Q40::YFP expression or neuronal *cco-1* KD compared with wild-type animals (Figure 2D). Likewise, PDI-6 protein levels were also elevated in animals with neuronal mitochondrial stresses (Figures 2E and 2F). Together, these results suggest that PDI-6 functions in Wnt/EGL-20-producing cells in response to neuronal mitochondrial stresses for cell-non-autonomous UPR^{mt} activation.

PDI-6 is required for Wnt/EGL-20 stability and gradient formation at adult stage

PDI family proteins catalyze cysteine-based redox reactions and play pivotal roles in oxidative protein folding accompanied by disulfide formation, as well as efficient ERAD accompanied by disulfide reduction (Braakman and Hebert, 2013; Okumura et al., 2015). In humans, there are more than 20 PDI family members, and each forms protein-protein interactions with preferred partners to fulfill distinct functions (Jessop et al., 2009). In *C. elegans*, the PDI family consists of five members (PDI-1, PDI-2, PDI-3, PDI-6, and C14B9.2). We found that none of the PDI family members other than PDI-6 were involved in cell-non-autonomous UPR^{mt} induction in animals with neuronal Wnt/EGL-20 overexpression (Figures S2A–S2D).

Because expression of *pdi-6* solely in Wnt/EGL-20-producing cells is sufficient to rescue the suppressed *hsp-6p*::*gfp* phenotype in *pdi-6* mutant animals with neuronal Q40::YFP expression, we next examined whether *pdi-6* is expressed in Wnt/EGL-20-producing cells. Marked by the *egl-20p*::*egl-20*::*mCherry* transgenic reporter, Wnt/EGL-20 is expressed in a group of cells in the tail of *C. elegans* (Zhang et al., 2018b). We found that the expression of *pdi-6*::*gfp* (CRISPR-mediated GFP knockin) is co-localized with the *egl-20p*::*egl-20*::*mCherry* reporter (Figure 3A).

Wnt proteins are rich in cysteines, and Wnt disulfide bond formation is essential for protein folding, maturation, and secretion (Braakman and Hebert, 2013; Feige and Hendershot, 2011). We therefore examined the stability and function of Wnt/EGL-20 in *pdi-6* mutants. The Wnt ligand EGL-20 is expressed by a group of cells in the tail and forms a posterior-to-anterior concentration gradient that can be visualized using an EGL-20::mCherry fusion protein reporter under the control of the *egl-20* native promoter (Zhang et al., 2018b).To observe whether the gradient of the Wnt ligand EGL-20 was affected by *pdi-6*, we introduced a *pdi-6(yth112)* mutation into a strain expressing the *egl-20p*::*egl-20*::*mCherry* reporter. In wild-type animals, EGL-20::mCherry was visible as a punctate pattern that ranged from the Wnt-producing cells in the tail to the mid-body region (Figure 3B). In the early larval L1 stage, the formation of an EGL-20 gradient along the anteroposterior axis was comparable between *pdi-6* mutants and wild-type animals (Figures 3B–3D). However, at day 1 (D1) of the adult stage, the Wnt/EGL-20 gradient formation was greatly diminished in *pdi-6* mutants compared with wild-type animals (Figures 3E and 3F). Immunoblots confirmed that the EGL-20 protein level was comparable between *pdi-6* mutants and wild-type animals at the early larval L1 stage but significantly decreased at day 1 of the adult stage (Figures 3G–3J). However, the transcription level of *egl-20* (indicated by the transcriptional reporter *egl-20p*::*mCherry*) was comparable between wild-type and *pdi-6* mutants (Figure S3A). Moreover, *pdi-6* deficiency did not affect the expression of Wnt secretion factor Wls/MIG-14, as visualized by the transgenic *egl-20p*::*mig-14*::*gfp* reporter (Figure S3B) (Zhang et al., 2018a). We hypothesized that loss of *pdi-6* would result in misfolded EGL-20, which might lead to its degradation via the ERAD. Indeed, blocking the ERAD pathway by knockout of *hrd-1*, the gene encoding an E3 ubiquitin ligase of the ERAD pathway, resulted in accumulation of Wnt/EGL-20::mCherry signals and restored the reduced protein level of Wnt/EGL-20::mCherry to higher than wild-type levels in *pdi-6* mutants (Figures 3E, and 3F, 3I and 3J). This indicated that the reduction of EGL-20 protein in *pdi-6* mutants may be due to the degradation of misfolded EGL-20 by the ER quality control pathway.

Wnt activation stabilizes the downstream transcriptional co-activator β-catenin/BAR-1, which translocates into the nucleus and promotes the expression of Wnt target genes (Clevers, 2006). We found that mRNA levels of some Wnt target genes were significantly decreased in *pdi-6* mutants, indicating impaired Wnt signaling in *pdi-6* mutants (Figure 3K; Table S1) (Gorrepati et al., 2015; Jackson et al., 2014). Wnt signaling controls various neurodevelopmental events, including neuron migration, neuronal polarity, and axon guidance (Coudreuse et al., 2006; Hilliard and Bargmann, 2006; Pan et al., 2006; Whangbo and Kenyon, 1999). EGL-20/Wnt morphogen acts as a repellent for hermaphrodite-specific neuron (HSN) migration during embryogenesis (Pan et al., 2006). We found that *pdi-6* mutants did not exhibit any defect in the HSN migration phenotype (Figures S3C–S3E). Furthermore, in *C. elegans*, left Q (QL) neuroblast lineages migrate posteriorly whereas right Q (QR)

(I) Immunoblot of *egl-20p*::*egl-20*::*mCherry* expression in D1 animals as indicated.
(J) Quantification of *egl-20p*::*egl-20*::*mCherry* levels as shown in (I).
(K) Quantification of mRNA levels of Wnt target genes in day 1 adult WT and *pdi-6(yth112)* mutant animals.
White dashed lines indicate the outline of a worm. White solid lines indicate the EGL-20-producing cells. Bold white dashed lines indicate the EGL-20 gradient. Scale bar, 10 μm. **p < 0.01; ***p < 0.001; ns, not significant (p > 0.05, t test). Error bars, SEM; n ≥ 3.
See also Figure S3.

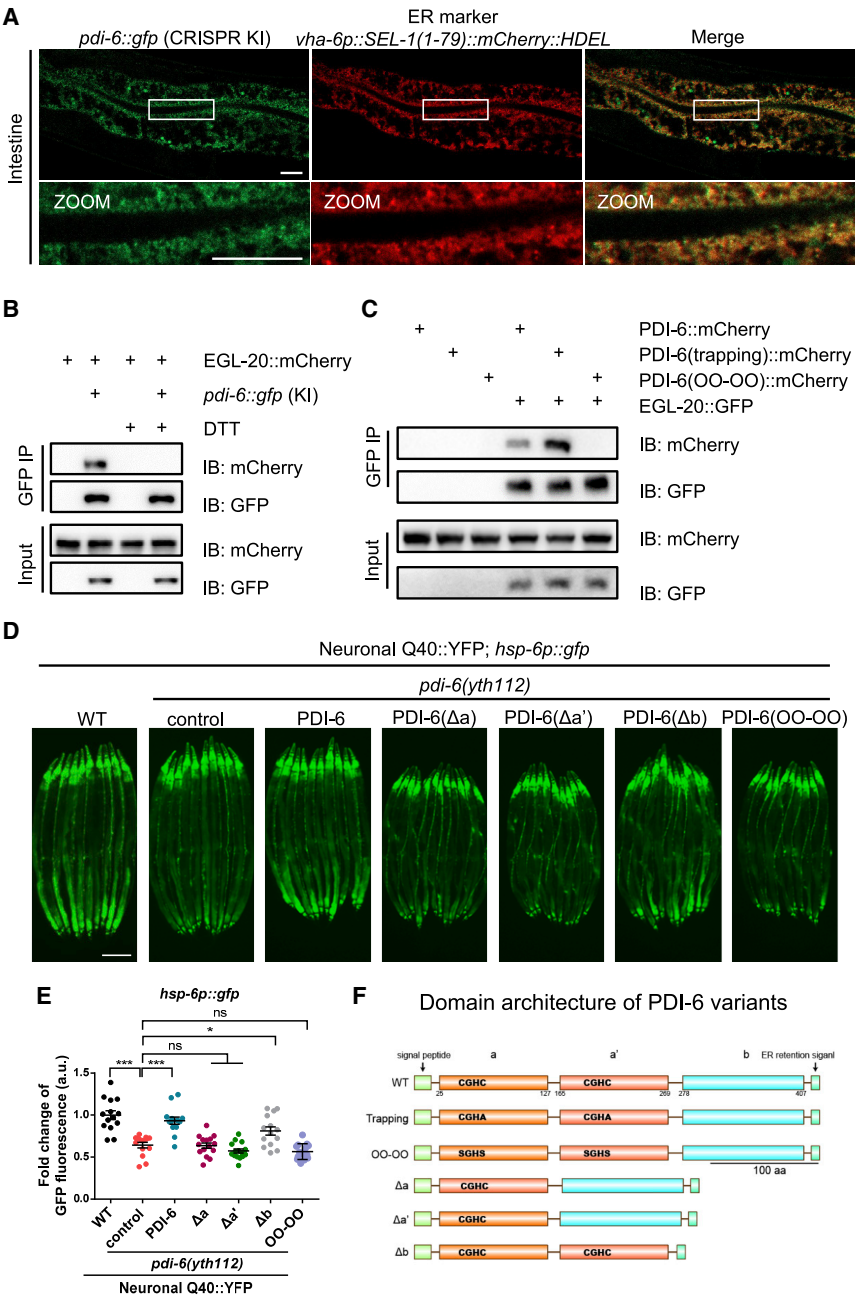

Figure 4. PDI-6 interacts with Wnt/EGL-20 potentially through intermolecular disulfide bonds

(A) Representative confocal photomicrographs of day 1 adult animals with *pdi-6*::*gfp* in combination with an intestinal ER luminal marker *vha-6p*::*SEL-1(1–79)*::*mcherry*::*HDEL*. Panels below show high-magnification views of boxed regions. Scale bar, 10 μm.

(B) WT animals expressing *egl-20p*::*egl-20*::*mCherry* with or without *pdi-6*::*gfp* were immunoprecipitated with GFP-trap agarose in the presence or absence of DTT. *pdi-6*::*gfp*-bound EGL-20::mCherry was detected by immunoblot.

(C) WT animals expressing *pdi-6p*::*pdi-6*::*mCherry*, *pdi-6p*::*pdi-6(trapping mutant)*::*mCherry*, or *pdi-6p*::*pdi-6(OO-OO)*::*mCherry* in the presence or absence of *egl-20p*::*egl-20*::*gfp* were immunoprecipitated with GFP-trap agarose. EGL-20::GFP-bound PDI-6::mCherry, PDI-6(trapping mutant)::mCherry, or PDI-6(OO-OO):mCherry was detected by immunoblot.

(D) Representative photomicrographs of *rgef-1p*::*Q40*::*yfp*, *hsp-6p*::*gfp*, and *pdi-6(yth112)* day 1 adult animals with or without *pdi-6p*::*pdi-6(Δa)*::*mCherry*, *pdi-6p*::*pdi-6(Δa')*::*mCherry*, *pdi-6p*::*pdi-6(Δb)*::*mCherry*, or *pdi-6p*::*pdi-6(OO-OO)*::*mCherry* expression as indicated. Scale bar, 250 μm.

(E) Quantification of *hsp-6p*::*gfp* expression as shown in (D). ***p < 0.001; ns, not significant (p > 0.05, t test). Error bars, SEM; n ≥ 15 worms.

(F) Schematic representation of the domain architecture of PDI-6 WT, single domain deletion version of PDI-6(Δa, Δa', and Δb), trapping mutant, and OO-OO variants. Scale bar, 100 amino acids (aa).

See also Figure S4.

PDI-6 interacts with Wnt/EGL-20 through disulfide-dependent association

Consistent with the previous report on PDIs (Eletto et al., 2014), the *pdi-6*::*gfp* signal is co-localized with the ER luminal marker *vha-6p*::*SEL-1(1–79)*::*mCherry*::*HDEL* in the intestine (Figure 4A) (Klemm et al., 2013). Despite the fact that some *pdi-6*::*gfp* signals had very close contact sites with mitochondria, we did not observe co-localization of *pdi-6*::*gfp* with the mitochondrial outer membrane marker *ges-1p*::*tomm-20*::*mKate2*::*HA* (Figure S4A) (Ahier et al., 2018). Additionally, we found no obvious co-localization of *pdi-6*::*gfp* with a lysosomal membrane marker *ced-1p*::*laat-1*::*mCherry* (Figure S4B) (Miao et al., 2020).

and its descendants migrate anteriorly (Whangbo and Kenyon, 1999). Loss of EGL-20/Wnt leads to abnormal migration of left Q neuroblast descendants (QL.ds) toward the anterior region during early larval development (Figure S3F) (Whangbo and Kenyon, 1999). However, *pdi-6* mutants showed a normal QL.ds migration phenotype (Figures S3G and S3H), suggesting that loss of *pdi-6* may not affect the developmental function of Wnt/EGL-20 during the early developmental stage. We thus found that canonical Wnt signaling was not significantly affected in *pdi-6* mutants during the early larval stage, but was specifically impaired in adulthood.

In humans, 19 WNT proteins have been identified that share 27% to 83% amino acid sequence identity and a conserved pattern of 23 or 24 cysteine residues; these form intramolecular disulfide bonds to maintain functional Wnt globular secondary structure (Miller, 2001; Willert and Nusse, 2012). Mutation of any individual cysteine in Wnt3a results in covalent Wnt oligomers through ectopic intermolecular disulfide bond formation,

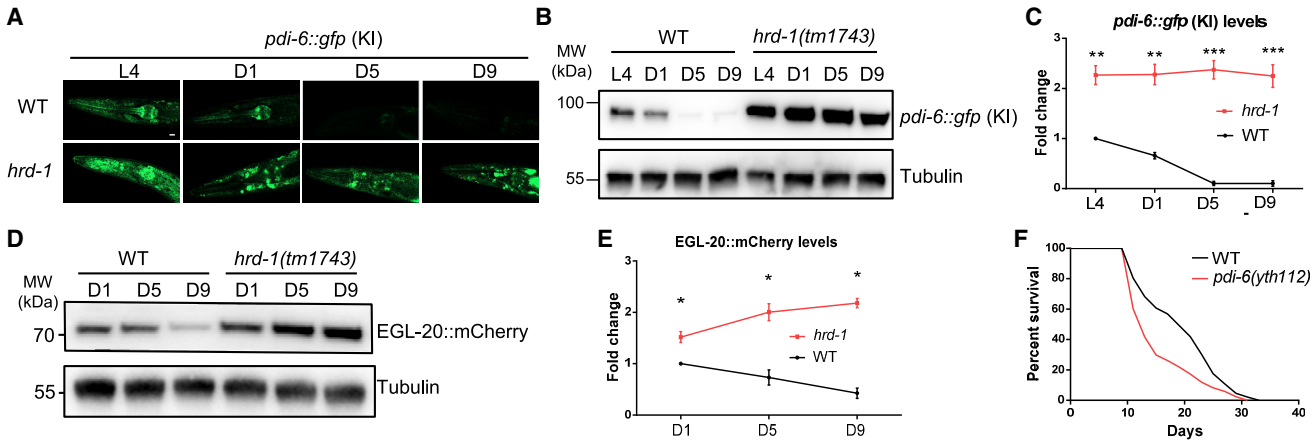

Figure 5. PDI-6 levels decline with age

(A) Representative confocal photomicrograph of animals expressing *pdi-6*::*gfp* in WT and *hrd-1(tm1743)* at different ages. Scale bar, 20 μm.

(B) Immunoblot of *pdi-6*::*gfp* in WT and *hrd-1(tm1743)* mutant animals at different ages.

(C) Quantification of *pdi-6*::*gfp* protein levels with age as shown in (B). The fold change represents *pdi-6*::*gfp* compared with tubulin and then each compared with WT L4. **p < 0.01; ***p < 0.001 (t test). Error bars, SEM; n ≥ 3.

(D) Immunoblot of *egl-20p*::*egl-20*::*mCherry* in WT and *hrd-1(tm1743)* mutant animals at different ages.

(E) Quantification of *egl-20p*::*egl-20*::*mCherry* protein levels with age as shown in (D). The fold change represents *egl-20p*::*egl-20*::*mCherry* compared with tubulin and then each compared with WT D1. *p < 0.05 (t test). Error bars, SEM; n ≥ 3.

(F) Survival analyses of WT and *pdi-6(yth112)* animals; n ≥ 100 worms.

See also Figure S5 and Table S2.

impairing Wnt secretion and activity (MacDonald et al., 2014). We therefore investigated whether PDI-6 interacts with EGL-20. Using the *pdi-6*::*gfp* knockin strain with the expression of EGL-20::mCherry, we performed an *in vivo* co-immunoprecipitation assay. Consistent with our hypothesis, PDI-6::GFP interacted with EGL-20::mCherry *in vivo* (Figure 4B). Moreover, addition of the reducing agent dithiothreitol (DTT) eliminated the interaction between PDI-6 and EGL-20 (Figure 4B), indicating that this interaction is largely dependent on the intramolecular or intermolecular disulfide bonds between PDI-6 and EGL-20.

To further understand whether PDI-6 interacts with EGL-20 through intermolecular disulfide bonds, we constructed a PDI-6 substrate-trapping mutant expression vector, where the second cysteine of each redox-active site was mutated to alanine (C39A; C146A) so that the substrate protein could be efficiently trapped in the complex (Jessop et al., 2009). Furthermore, there are two enzymatic CGHC motifs in the PDI-6 protein that are critical for enzymatic function of PDI-6. Therefore, we constructed a catalytic cysteine-free variant of PDI-6, PDI-6(OO-OO), as the two pairs of sulfurs in the cysteines of the active site were mutated to oxygens in the resulting serines (C37S, C39S; C144S, C146S) (Zhou et al., 2015). Consistent with our expectations, the interaction between PDI-6 and EGL-20 was strengthened in the substrate-trapping mutant PDI-6, and the interaction disappeared when PDI-6(OO-OO) was used (Figure 4C). Furthermore, we prepared worm lysates in the presence of *N*-ethylmaleimide (NEM) to quench free thiols, and protein complexes were immunoprecipitated by the GFP-trap agarose. Immunoblot of a non-reducing gel showed that PDI-6(trapping mutant)::mCherry was associated with EGL-20::GFP in a high-molecular-disulfide-bonded complex, and a species of similar mobility was also detected with the anti-GFP antibody (Figure S4C). These data suggest that PDI-6 interacts with EGL-20 *in vivo* and that this interaction is largely dependent on the intermolecular disulfide bonds formed between PDI-6 and EGL-20, since PDI-6(OO-OO) does not interact with EGL-20 (Figure S4C).

PDI-6 consists of three thioredoxin-like domains, the a, a′, and b domains, resembling mammalian PDIA6. To further investigate which domain is essential for PDI-6 regulation of cell-non-autonomous UPR^{mt}, we constructed three different truncated forms of PDI-6. Each was depleted in a single domain, and the mutants were correspondingly called Δa, Δa′, and Δb. Intriguingly, expression of PDI-6(Δb) partially rescued the suppression of *hsp-6p*::*gfp* in *pdi-6* mutants, whereas expression of PDI-6(Δa) or PDI-6(Δa′) could not rescue the suppression of *hsp-6p*::*gfp* in *pdi-6* mutants (Figures 4D–4F), suggesting that a and a′ domains are indispensable for PDI-6 in UPR^{mt} regulation. Furthermore, the non-catalytically functional PDI-6(OO-OO) could not rescue the suppressed *hsp-6p*::*gfp* in *pdi-6* mutants, indicating the disulfide bond catalytic function is essential for PDI-6 in the regulation of cell-non-autonomous UPR^{mt} (Figures 4D–4F).

Levels of PDI-6 and Wnt/EGL-20 decrease with age, and *pdi-6* deficiency shortens lifespan

PDIs have broad implications in physiology and pathology (Honjo et al., 2017; Kaplan et al., 2015; Oka et al., 2013; Perri et al., 2016; Uehara et al., 2006; Ushioda et al., 2008; Zhou et al., 2018). To investigate the role of PDI-6 in the aging process, we first measured the protein level of PDI-6 during aging. We observed that *pdi-6*::*gfp* levels dropped off between L4 and D5 and then stay the same (Figures 5A–5C). Because misfolded proteins tend to accumulate with age, causing activation of the ERAD pathway, we hypothesized that age-related proteostasis

dysregulation might lead to degradation of PDI-6 via the ERAD pathway. Indeed, we found that loss of *hrd-1* increased and maintained PDI-6 protein levels during aging (Figures 5A–5C), indicating that PDI-6 is degraded through the ERAD during aging. Furthermore, we found that the Wnt/EGL-20 level also decreased with age in an ERAD-dependent manner (Figures 5D and 5E). In contrast, the mRNA levels of *egl-20* and *pdi-6* increased with age (Figure S5A), suggesting there may exist a feedback regulation due to the decline of protein level. The median lifespan of *pdi-6(yth112)* mutants was shorter than that of wild-type animals, whereas the maximal lifespan was not significantly affected (Figure 5F; Table S2).

Overexpression of PDI-6 is sufficient to maintain Wnt/EGL-20 levels during aging and extends lifespan in a Wnt- and UPR^{mt}-dependent manner

To investigate whether PDI-6 overexpression is sufficient to induce UPR^{mt}, we overexpressed PDI-6 in animals expressing the UPR^{mt} reporter *hsp-6p*::*gfp*. We found that overexpression of PDI-6 was sufficient to activate intestinal UPR^{mt} in a Wnt/EGL-20 signaling-dependent manner (Figures 6A and 6B). Because the protein level of *pdi-6*::*gfp* declined with age, we asked whether increasing PDI-6 protein levels could maintain Wnt/EGL-20 stability during aging. We found that PDI-6 overexpression maintained Wnt/EGL-20 protein levels with age (Figures 6C and 6D). Furthermore, overexpression of PDI-6 significantly extended lifespan in *C. elegans* (Figure 6E; Table S2), and the lifespan extension effect disappeared when overexpressing the catalytic cysteine-free PDI-6(OO-OO) (Figure 6F; Table S2), suggesting that the catalytic function of PDI-6 is critical for lifespan regulation.

To investigate whether PDI-6 overexpression extends lifespan through Wnt signaling, UPR^{mt}, or UPR^{ER}, we introduced *egl-20(n585)*, *atfs-1(gk3094)*, and *xbp-1(tm2482)* mutations into the PDI-6 overexpression strain. Lifespan extension was not observed in *egl-20* and *atfs-1* mutants but was present in *xbp-1* mutants (Figures 6G–6I; Table S2), indicating that Wnt signaling and UPR^{mt} are required for PDI-6-induced lifespan extension. PDI-6 acts as a coordinator of intercellular mitochondrial stress signaling; we thus asked whether overexpressing PDI-6 in neurons could induce intestinal UPR^{mt} and extend lifespan as well. We found that overexpressing PDI-6 in neurons was sufficient to induce intestinal UPR^{mt} and longevity in a Wnt/EGL-20-signaling-dependent manner (Figures S6A–S6E; Table S2). Furthermore, overexpressing PDI-6 in the intestine, the epidermis, or the body wall muscle could also extend lifespan to some extent (Figures S6F–S6H; Table S2). These results demonstrate a significant role for PDI-6 in lifespan regulation.

It has been reported that PDIA6, the mammalian homolog of PDI-6, limits excessive UPR^{ER} signaling; PDIA6-deficient cells are hyper-responsive to ER stress, resulting in increased apoptosis (Eletto et al., 2014). To investigate whether PDI-6 plays a similar protective role against multiple stresses in *C. elegans*, we treated animals overexpressing PDI-6 with paraquat (oxidative stress), DTT (reductive stress), tunicamycin (ER stress), or CCCP (carbonyl cyanide 3-chlorophenylhydrazone, mitochondrial stress). Animals overexpressing PDI-6 exhibited significant resistance to oxidative stress (Figure 6J; Table S2). However, they were more sensitive to reductive stress, which may disrupt the disulfide bonds in PDI-6 (Figure 6K; Table S2). Furthermore, we found that animals overexpressing PDI-6 displayed high resistance to tunicamycin (ER stress) and CCCP (mitochondrial stress) (Figures 6L and 6M). These results implicate PDI-6 as a critical protector against multiple stresses.

DISCUSSION

Wnt proteins are morphogens forming concentration gradients to control cell proliferation, stem cell maintenance, differentiation, neuronal migration, developmental patterning, and tissue regeneration (Nusse and Clevers, 2017; Reya and Clevers, 2005; Wodarz and Nusse, 1998). Aberrant Wnt activation has been associated with a variety of cancer types, and Wnt signaling function has been proposed to be protective against neurodegenerative diseases (Inestrosa and Arenas, 2010; Logan and Nusse, 2004). However, the mechanisms underlying regulation of Wnt protein folding and maturation to enable Wnt secretion and long-range signaling have remained elusive. We here showed that EGL-20 stability is controlled by the protein disulfide isomerase PDI-6, potentially through disulfide bond catalytic activity, to coordinate inter-tissue proteostasis, which can help maintain organismal health during the aging process (Figure 7).

Intercellular signaling may have evolved to enable animals to sense extrinsic environmental signals and then amplify those signals across the entire animal to coordinate appropriate onset of development, reproduction, or aging. Numerous studies have demonstrated that tissue-specific manipulation of several conserved signaling pathways, such as the insulin/IGF-1 or Wnt signaling pathways, could affect homeostasis or even aging of the entire organism (Hwangbo et al., 2004; Libina et al., 2003; Wolkow et al., 2000; Zhang et al., 2018b). A previous study showed that retromer-mediated Wnt signaling is required for neuron-to-intestine UPR^{mt} signaling (Zhang et al., 2018b). However, it remains unclear whether or how neuronal mitochondrial stress can activate Wnt signaling and induce UPR^{mt} over a distance. Here, we have shown that the protein disulfide isomerase PDI-6 is upregulated in response to neuronal mitochondrial stress and that expressing PDI-6 in pan-neurons or solely EGL-20-producing cells is necessary for cell-non-autonomous UPR^{mt} communication. Our results indicate that PDI-6 is required to propagate Wnt signaling in response to neuronal mitochondrial stress to maintain organismal mitochondrial proteostasis.

The structures of complex Wnt family proteins are coordinated by intramolecular disulfide bonds formed between conserved cysteine residues (Willert and Nusse, 2012). Although past experiments did not find any secretory proteins in PDIA6 clients by either physical association or functional assays (Eletto et al., 2014; Jessop et al., 2009; Rutkevich et al., 2010), recent research has shown that PDIA6 is cell-extrinsically required for lymphoid and myeloid development and is required for Wnt3a folding and subsequent secretion (Choi et al., 2020). Moreover, PDI-1 has been demonstrated to affect Wnt/EGL-20-directing HSN migration during embryogenesis (Torpe et al., 2019), but it is not required for the Wnt-dependent mitokine signaling. Here, we

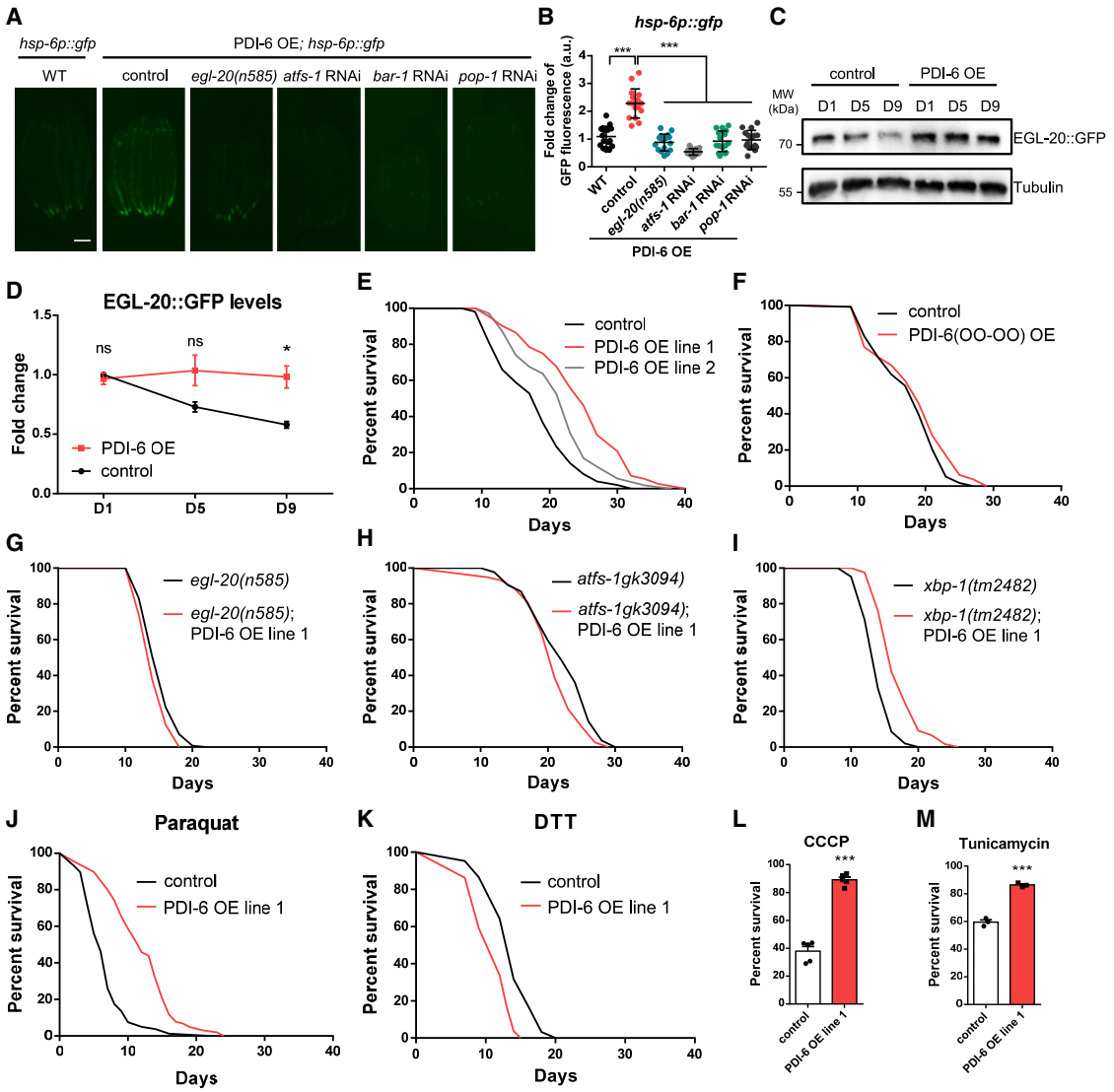

Figure 6. Overexpression of PDI-6 maintains Wnt/EGL-20 levels during aging and induces intestinal UPR^{mt} and longevity in a Wnt/EGL-20-dependent manner

(A) Representative photomicrograph of day 1 adult animals expressing *hsp-6p*::*gfp* and *pdi-6p*::*pdi-6*::*mCherry* in WT, *egl-20(n585)*, *atfs-1* RNAi, *bar-1* RNAi, and *pop-1* RNAi. Scale bar, 250 μm.

(B) Quantification of *hsp-6p*::*gfp* expression as shown in (A). ***$p < 0.001$ (t test). Error bars, SEM; $n \geq 15$ worms.

(C) Immunoblot of *egl-20p*::*egl-20*::*gfp* in control and *pdi-6p*::*pdi-6*::*mCherry*-overexpressing animals at different ages.

(D) Quantification of *egl-20p*::*egl-20*::*gfp* protein levels as shown in (C). *$p < 0.05$; ns, not significant ($p > 0.05$, t test). Error bars, SEM; $n \geq 3$.

(E) Survival analysis of two independent transgenic lines of animals with *pdi-6p*::*pdi-6*::*mCherry* overexpression; $n \geq 100$ worms.

(F) Survival analyses of WT animals and animals with *pdi-6p*::*pdi-6(OO-OO)*::*mCherry* overexpression; $n \geq 100$ worms.

(G) Survival analyses of *egl-20(n585)* mutant animals and *egl-20(n585)*; *pdi-6p*::*pdi-6*::*mCherry* animals; $n \geq 100$ worms.

(H) Survival analyses of *atfs-1(gk3094)* and *pdi-6p*::*pdi-6*::*mCherry*; *atfs-1(gk3094)* animals; $n \geq 100$ worms.

(I) Survival analyses of *xbp-1(tm2482)* and *pdi-6p*::*pdi-6*::*mCherry*; *xbp-1(tm2482)* animals; $n \geq 100$ worms.

(J) Survival analyses of WT animals and animals expressing *pdi-6p*::*pdi-6*::*mCherry* transferred to nematode growth medium (NGM) plates containing 5 mM paraquat from young adult stage; $n \geq 100$ worms.

(K) Survival analyses of WT animals and animals expressing *pdi-6p*::*pdi-6*::*mCherry* transferred to NGM plates containing 5 mM DTT from young adult stage; $n \geq 100$ worms.

(L) Survival rates of day 1 adult WT animals and animals expressing *pdi-6p*::*pdi-6*::*mCherry* after treatment with 200 μM CCCP for 3.5 h. ***$p < 0.001$ (t test). Error bars, SEM; $n \geq 3$.

(M) Survival rates of day 1 adult WT animals and animals expressing *pdi-6p*::*pdi-6*::*mCherry* after treatment with 100 ng/μL tunicamycin for 20 h. ***$p < 0.001$ (t test). Error bars, SEM; $n \geq 3$.

See also Figure S6 and Table S2.

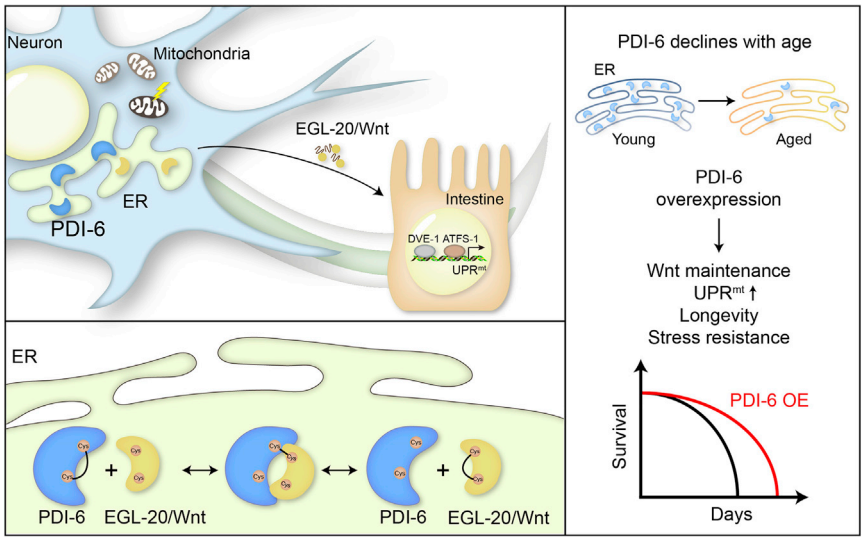

Figure 7. Schematic model of PDI-6 regulating inter-tissue UPR^{mt} and lifespan via Wnt signaling

PDI-6 coordinates the inter-tissue UPR^{mt} signaling by assisting the Wnt ligand EGL-20 secretion. PDI-6 drastically declines with aging, and overexpression PDI-6 confers stress resistance and longevity.

have demonstrated that PDI-6 is specifically required for cell-non-autonomous UPR^{mt} communication by regulating Wnt/EGL-20 stability in *C. elegans* using a genetic screen.

Wnt signaling has been associated with aging. In intestine stem cells (ISCs), canonical Wnt signaling declines, which leads to decreased ISC regenerative potential. Exogenous Wnts supplementation *in vitro* ameliorates aging and improves regeneration of aged ISCs (Nalapareddy et al., 2017; Pentinmikko et al., 2019). Here, we have shown that Wnt/EGL-20 levels decrease with age in an ERAD-dependent manner. Furthermore, overexpressing PDI-6 is sufficient to maintain Wnt/EGL-20 protein levels during aging, activating UPR^{mt} and inducing longevity in a Wnt/EGL-20-dependent manner.

PDIs are critical for proper maintenance of ER protein homeostasis to avoid cellular stresses and diseases caused by abnormal proteins (Eletto et al., 2014; Oka et al., 2013; Uehara et al., 2006; Ushioda et al., 2008). Dysfunctional PDI is associated with neurodegenerative diseases, such as Alzheimer's disease and Parkinson's disease (Honjo et al., 2017; Kaplan et al., 2015; Perri et al., 2016; Zhou et al., 2018). Aberrant PDI activity leads to protein misfolding- and aggregation-related pathology (Uehara et al., 2006). In human mesenchymal stem cells derived from bone marrow, the expression of PDIA6 declines with cellular senescence (Yoo et al., 2013). Here, we have demonstrated that levels of PDI-6 significantly decline with aging, implicating impaired protein folding and secretion capacity of the ER in the aging process. Additionally, we have shown that overexpression of PDI-6 extends lifespan in a Wnt/EGL-20- and UPR^{mt}-dependent manner in *C. elegans*. Further studies of the relationship between PDI and aging may lead to discovery of potential therapeutic interventions in aging and age-related diseases.

In summary, we discovered that a specific protein disulfide isomerase, PDI-6, is required for Wnt-dependent mitokine signaling, potentially via catalyzing disulfide bond formation for Wnt activity. Furthermore, our study linked PDI, Wnt signaling, UPR^{mt}, and aging, making it an appealing future target for therapeutic interventions in aging and age-related diseases.

Limitations of the study

The main challenge of this study was to analyze disulfide bond formation of Wnt/EGL-20 in animals with *pdi-6* deficiency, since Wnt is lipid modified and poorly water soluble. In addition, we used an unbiased genetic screen to identify that PDI-6 mediates Wnt/EGL-20 stability and secretion. We do not know whether PDI family members promote disulfide bond formation for other Wnt proteins.

STAR★METHODS

Detailed methods are provided in the online version of this paper and include the following:

- KEY RESOURCES TABLE
- RESOURCE AVAILABILITY
  - Lead contact
  - Materials availability
  - Data and code availability
- EXPERIMENTAL MODEL AND SUBJECT DETAILS
  - *Caenorhabditis elegans* maintenance
- METHOD DETAILS
  - EMS mutagenesis screen
  - Gene mapping
  - Generation of different alleles of *pdi-6* mutants
  - RNAi feeding
  - Co-immunoprecipitation
  - Heat shock assay
  - Transgenic strain construction
  - Examination of QL.d and HSN migration
  - Analysis of the fluorescence intensity in whole worm
  - Western Blot analysis
  - Antibodies
  - RNA isolation and quantitative PCR analyses
  - Lifespan analysis
  - Tunicamycin killing assay
  - CCCP killing assay
- QUANTIFICATION AND STATISTICAL ANALYSIS

SUPPLEMENTAL INFORMATION

Supplemental information can be found online at https://doi.org/10.1016/j.celrep.2022.110931.

ACKNOWLEDGMENTS

We thank Tian laboratory members for insightful discussions and Yating Liu for helping with strain maintenance. Several *C. elegans* strains used in this work were provided by the Caenorhabditis Genetics Center (CGC), which is supported by the NIH-Officer of Research Infrastructure Programs (P40 OD010440) and the Japanese National BioResource Project. The LAAT-1 lysosomal marker strain and MIG-14 reporter strain were kindly provided by Dr. Xiaochen Wang's laboratory. Y.T. was supported by the National Key R&D Program of China (2017YFA0506400), the National Natural Science Foundation of China (31930023), and the Strategic Priority Research Program of the Chinese Academy of Sciences (XDB39000000). X.W. was supported by the Youth Innovation Promotion Association CAS (2021094). Q.Z. was supported by the China National Postdoctoral Program for Innovative Talents (BX2021356).

AUTHOR CONTRIBUTIONS

Y.T. and X.L. conceived the study and wrote the manuscript; Q.Z., Y.L., and X.L. performed the genetic screen and outcrosses; X.L. isolated the *pdi-6(yth16)* mutants, made the transgene constructs, and performed the RNAi experiments; X.L. and X.W. performed the immunoprecipitation experiments; X.L. and J.L. performed the *C. elegans* crosses, strain generations, western blotting, drug treatment, and fluorescence microscopy experiments; X.L., X.H., D.Z., and J.L. performed the lifespan experiments; X.L., N.Z., J.L., and W.Z. performed the microinjection experiments.

DECLARATION OF INTERESTS

The authors declare no competing interests.

Received: September 28, 2021
Revised: March 2, 2022
Accepted: May 18, 2022
Published: June 7, 2022

REFERENCES

Ahier, A., Dai, C.Y., Tweedie, A., Bezawork-Geleta, A., Kirmes, I., and Zuryn, S. (2018). Affinity purification of cell-specific mitochondria from whole animals resolves patterns of genetic mosaicism. Nat. Cell Biol. *20*, 352–360. https://doi.org/10.1038/s41556-017-0023-x.

Arata, Y., Kouike, H., Zhang, Y., Herman, M.A., Okano, H., and Sawa, H. (2006). Wnt signaling and a Hox protein cooperatively regulate PSA-3/Meis to determine daughter cell fate after asymmetric cell division in *C. elegans*. Dev. Cell *11*, 105–115. https://doi.org/10.1016/j.devcel.2006.04.020.

Berendzen, K.M., Durieux, J., Shao, L.W., Tian, Y., Kim, H., Wolff, S., Liu, Y., and Dillin, A. (2016). Neuroendocrine coordination of mitochondrial stress signaling and proteostasis. Cell *166*, 1553–1563.e10. https://doi.org/10.1016/j.cell.2016.08.042.

Braakman, I., and Hebert, D.N. (2013). Protein folding in the endoplasmic reticulum. Cold Spring Harb. Perspect. Biol. *5*, a013201. https://doi.org/10.1101/cshperspect.a013201.

Brignull, H.R., Moore, F.E., Tang, S.J., and Morimoto, R.I. (2006). Polyglutamine proteins at the pathogenic threshold display neuron-specific aggregation in a pan-neuronal *Caenorhabditis elegans* model. J. Neurosci. *26*, 7597–7606. https://doi.org/10.1523/jneurosci.0990-06.2006.

Calfon, M., Zeng, H., Urano, F., Till, J.H., Hubbard, S.R., Harding, H.P., Clark, S.G., and Ron, D. (2002). IRE1 couples endoplasmic reticulum load to secretory capacity by processing the XBP-1 mRNA. Nature *415*, 92–96. https://doi.org/10.1038/415092a.

Chen, L.T., Lin, C.T., Lin, L.Y., Hsu, J.M., Wu, Y.C., and Pan, C.L. (2021). Neuronal mitochondrial dynamics coordinate systemic mitochondrial morphology and stress response to confer pathogen resistance in *C. elegans*. Dev. Cell *56*, 1770–1785.e12. https://doi.org/10.1016/j.devcel.2021.04.021.

Choi, J.H., Zhong, X., Zhang, Z., Su, L., McAlpine, W., Misawa, T., Liao, T.C., Zhan, X., Russell, J., Ludwig, S., et al. (2020). Essential cell-extrinsic requirement for PDIA6 in lymphoid and myeloid development. J. Exp. Med. *217*, 1–13. https://doi.org/10.1084/jem.20190006.

Clevers, H. (2006). Wnt/β-catenin signaling in development and disease. Cell *127*, 469–480. https://doi.org/10.1016/j.cell.2006.10.018.

Copeland, J.M., Cho, J., Lo, T., Hur, J.H., Bahadorani, S., Arabyan, T., Rabie, J., Soh, J., and Walker, D.W. (2009). Extension of *Drosophila* life span by RNAi of the mitochondrial respiratory chain. Curr. Biol. *19*, 1591–1598. https://doi.org/10.1016/j.cub.2009.08.016.

Coudreuse, D.Y.M., Roël, G., Betist, M.C., Destrée, O., and Korswagen, H.C. (2006). Wnt gradient formation requires retromer function in Wnt-producing cells. Science *312*, 921–924. https://doi.org/10.1126/science.1124856.

Davis, M.W., Hammarlund, M., Harrach, T., Hullett, P., Olsen, S., and Jorgensen, E.M. (2005). Rapid single nucleotide polymophism mapping in *C. elegans*. BMC Genom. *6*, 118–211. https://doi.org/10.1186/1471-2164-6-118.

Dillin, A., Hsu, A.L., Arantes-Oliveira, N., Lehrer-Graiwer, J., Hsin, H., Fraser, A.G., Kamath, R.S., Ahringer, J., and Kenyon, C. (2002). Rates of behavior and aging specified by mitochondrial function during development. Science *298*, 2398–2401. https://doi.org/10.1126/science.1077780.

Douglas, P.M., Baird, N.A., Simic, M.S., Uhlein, S., McCormick, M.A., Wolff, S.C., Kennedy, B.K., and Dillin, A. (2015). Heterotypic signals from neural HSF-1 separate thermotolerance from longevity. Cell Rep. *12*, 1196–1204. https://doi.org/10.1016/j.celrep.2015.07.026.

Durieux, J., Wolff, S., and Dillin, A. (2011). The cell-non-autonomous nature of electron transport chain-mediated longevity. Cell *144*, 79–91. https://doi.org/10.1016/j.cell.2010.12.016.

Eletto, D., Eletto, D., Dersh, D., Gidalevitz, T., and Argon, Y. (2014). Protein disulfide isomerase A6 controls the decay of IRE1α signaling via disulfide-dependent association. Mol. Cell *53*, 562–576. https://doi.org/10.1016/j.molcel.2014.01.004.

Feige, M.J., and Hendershot, L.M. (2011). Disulfide bonds in ER protein folding and homeostasis. Curr. Opin. Cell Biol. *23*, 167–175. https://doi.org/10.1016/j.ceb.2010.10.012.

Feng, J., Bussière, F., and Hekimi, S. (2001). Mitochondrial electron transport is a key determinant of life span in *Caenorhabditis elegans*. Dev. Cell *1*, 633–644. https://doi.org/10.1016/s1534-5807(01)00071-5.

Frakes, A.E., and Dillin, A. (2017). The UPR^{ER}: sensor and coordinator of organismal homeostasis. Mol. Cell *66*, 761–771. https://doi.org/10.1016/j.molcel.2017.05.031.

Goldstein, B., Takeshita, H., Mizumoto, K., and Sawa, H. (2006). Wnt signals can function as positional cues in establishing cell polarity. Dev. Cell *10*, 391–396. https://doi.org/10.1016/j.devcel.2005.12.016.

Gorrepati, L., Krause, M.W., Chen, W., Brodigan, T.M., Correa-Mendez, M., and Eisenmann, D.M. (2015). Identification of wnt pathway target genes regulating the division and differentiation of larval seam cells and vulval precursor cells in *Caenorhabditis elegans*. G3 Genes, Genomes, Genet. *5*, 1551–1566. https://doi.org/10.1534/g3.115.017715.

Haynes, C.M., Petrova, K., Benedetti, C., Yang, Y., and Ron, D. (2007). ClpP mediates activation of a mitochondrial unfolded protein response in *C. elegans*. Dev. Cell *13*, 467–480. https://doi.org/10.1016/j.devcel.2007.07.016.

Haynes, C.M., Yang, Y., Blais, S.P., Neubert, T.A., and Ron, D. (2010). The matrix peptide exporter HAF-1 signals a mitochondrial UPR by activating the transcription factor ZC376.7 in *C. elegans*. Mol. Cell *37*, 529–540. https://doi.org/10.1016/j.molcel.2010.01.015.

Hilliard, M.A., and Bargmann, C.I. (2006). Wnt signals and Frizzled activity orient anterior-posterior axon outgrowth in *C. elegans*. Dev. Cell *10*, 379–390. https://doi.org/10.1016/j.devcel.2006.01.013.

Honjo, Y., Ayaki, T., Tomiyama, T., Horibe, T., Ito, H., Mori, H., Takahashi, R., and Kawakami, K. (2017). Decreased levels of PDI and P5 in oligodendrocytes in Alzheimer's disease. Neuropathology *37*, 495–501. https://doi.org/10.1111/neup.12395.

Hwangbo, D.S., Gersham, B., Tu, M.P., Palmer, M., and Tatar, M. (2004). *Drosophila* dFOXO controls lifespan and regulates insulin signalling in brain and fat body. Nature *429*, 562–566. https://doi.org/10.1038/nature02549.

Inestrosa, N.C., and Arenas, E. (2010). Emerging roles of Wnts in the adult nervous system. Nat. Rev. Neurosci. *11*, 77–86. https://doi.org/10.1038/nrn2755.

Jackson, B.M., Abete-Luzi, P., Krause, M.W., and Eisenmann, D.M. (2014). Use of an activated beta-catenin to identify wnt pathway target genes in *Caenorhabditis elegans*, including a subset of collagen genes expressed in late larval development. G3 Genes, Genomes, Genet. *4*, 733–747. https://doi.org/10.1534/g3.113.009522.

Jessop, C.E., Watkins, R.H., Simmons, J.J., Tasab, M., and Bulleid, N.J. (2009). Protein disulphide isomerase family members show distinct substrate specificity: P5 is targeted to BiP client proteins. J. Cell Sci. *122*, 4287–4295. https://doi.org/10.1242/jcs.059154.

Kang, G.M., Min, S.H., Lee, C.H., Kim, J.Y., Lim, H.S., Choi, M.J., Jung, S.B., Park, J.W., Kim, S., Park, C.B., et al. (2021). Mitohormesis in hypothalamic POMC neurons mediates regular exercise-induced high-turnover metabolism. Cell Metabol. *33*, 334–349.e6. https://doi.org/10.1016/j.cmet.2021.01.003.

Kaplan, A., Gaschler, M.M., Dunn, D.E., Colligan, R., Brown, L.M., Palmer, A.G., Lo, D.C., and Stockwell, B.R. (2015). Small molecule-induced oxidation of protein disulfide isomerase is neuroprotective. Proc. Natl. Acad. Sci. U S A. *112*, e2245–e2252. https://doi.org/10.1073/pnas.1500439112.

Klemm, R.W., Norton, J.P., Cole, R.A., Li, C.S., Park, S.H., Crane, M.M., Li, L., Jin, D., Boye-Doe, A., Liu, T.Y., et al. (2013). A conserved role for atlastin GTPases in regulating lipid droplet size. Cell Rep. *3*, 1465–1475. https://doi.org/10.1016/j.celrep.2013.04.015.

Li, T.Y., Sleiman, M.B., Li, H., Gao, A.W., Mottis, A., Bachmann, A.M., Alam, G.E., Li, X., Goeminne, L.J.E., Schoonjans, K., and Auwerx, J. (2021). The transcriptional coactivator CBP/p300 is an evolutionarily conserved node that promotes longevity in response to mitochondrial stress. Nat. Aging *1*, 165–178. https://doi.org/10.1038/s43587-020-00025-z.

Libina, N., Berman, J.R., Kenyon, C., Hall, M.B.G., and Francisco, S. (2003). Tissue-specific activities of *C. elegans* DAF-16 in the regulation of lifespan. Cell *115*, 489–502. https://doi.org/10.1016/s0092-8674(03)00889-4.

Link, C.D., Cypser, J.R., Johnson, C.J., and Johnson, T.E. (1999). Direct observation of stress response in *Caenorhabditis elegans* using a reporter transgene. Cell Stress Chaperones *4*, 235–242. https://doi.org/10.1379/1466-1268(1999)004<0235:doosri>2.3.co;2.

Liu, X., Jiang, N., Hughes, B., Bigras, E., Shoubridge, E., and Hekimi, S. (2005). Evolutionary conservation of the clk-1-dependent mechanism of longevity: loss of mclk1 increases cellular fitness and lifespan in mice. Genes Dev. *19*, 2424–2434. https://doi.org/10.1101/gad.1352905.

Logan, C.Y., and Nusse, R. (2004). The Wnt signaling pathway in development and disease. Annu. Rev. Cell Dev. Biol. *20*, 781–810. https://doi.org/10.1146/annurev.cellbio.20.010403.113126.

MacDonald, B.T., Hien, A., Zhang, X., Iranloye, O., Virshup, D.M., Waterman, M.L., and He, X. (2014). Disulfide bond requirements for active Wnt ligands. J. Biol. Chem. *289*, 18122–18136. https://doi.org/10.1074/jbc.m114.575027.

Merkwirth, C., Jovaisaite, V., Durieux, J., Matilainen, O., Jordan, S.D., Quiros, P.M., Steffen, K.K., Williams, E.G., Mouchiroud, L., Tronnes, S.U., et al. (2016). Two conserved histone demethylases regulate mitochondrial stress-induced longevity. Cell *165*, 1209–1223. https://doi.org/10.1016/j.cell.2016.04.012.

Miao, R., Li, M., Zhang, Q., Yang, C., and Wang, X. (2020). An ECM-to-nucleus signaling pathway activates lysosomes for *C. elegans* larval development. Dev. Cell *52*, 21–37.e5. https://doi.org/10.1016/j.devcel.2019.10.020.

Miller, J.R. (2001). The wnts. Genome Biol. *10*, 235.1–235.7.

Mizumoto, K., and Sawa, H. (2007). Cortical β-catenin and APC regulate asymmetric nuclear β-catenin localization during asymmetric cell division in *C. elegans*. Dev. Cell *12*, 287–299. https://doi.org/10.1016/j.devcel.2007.01.004.

Morley, J.F., Brignull, H.R., Weyers, J.J., and Morimoto, R.I. (2002). The threshold for polyglutamine-expansion protein aggregation and cellular toxicity is dynamic and influenced by aging in *Caenorhabditis elegans*. Proc. Natl. Acad. Sci. U S A. *99*, 10417–10422. https://doi.org/10.1073/pnas.152161099.

Nalapareddy, K., Nattamai, K.J., Kumar, R.S., Karns, R., Wikenheiser-Brokamp, K.A., Sampson, L.L., Mahe, M.M., Sundaram, N., Yacyshyn, M.B., Yacyshyn, B., et al. (2017). Canonical Wnt signaling ameliorates aging of intestinal stem cells. Cell Rep. *18*, 2608–2621. https://doi.org/10.1016/j.celrep.2017.02.056.

Nargund, A.M., Pellegrino, M.W., Fiorese, C.J., Baker, B.M., and Haynes, C.M. (2012). Mitochondrial import efficiency of ATFS-1 regulates mitochondrial UPR activation. Science *337*, 587–590. https://doi.org/10.1126/science.1223560.

Nusse, R., and Clevers, H. (2017). Wnt/β-Catenin signaling, disease, and emerging therapeutic modalities. Cell *169*, 985–999. https://doi.org/10.1016/j.cell.2017.05.016.

Oka, O.B.V., Pringle, M.A., Schopp, I.M., Braakman, I., and Bulleid, N.J. (2013). ERdj5 is the ER reductase that catalyzes the removal of non-native disulfides and correct folding of the LDL receptor. Mol. Cell *50*, 793–804. https://doi.org/10.1016/j.molcel.2013.05.014.

Okumura, M., Kadokura, H., and Inaba, K. (2015). Structures and functions of protein disulfide isomerase family members involved in proteostasis in the endoplasmic reticulum. Free Radic. Biol. Med. *83*, 314–322. https://doi.org/10.1016/j.freeradbiomed.2015.02.010.

Owusu-Ansah, E., Song, W., and Perrimon, N. (2013). Muscle mitohormesis promotes longevity via systemic repression of insulin signaling. Cell *155*, 699–712. https://doi.org/10.1016/j.cell.2013.09.021.

Pan, C.L., Howell, J.E., Clark, S.G., Hilliard, M., Cordes, S., Bargmann, C.I., and Garriga, G. (2006). Multiple Wnts and Frizzled receptors regulate anteriorly directed cell and growth cone migrations in *Caenorhabditis elegans*. Dev. Cell *10*, 367–377. https://doi.org/10.1016/j.devcel.2006.02.010.

Pentinmikko, N., Iqbal, S., Mana, M., Andersson, S., Cognetta, A.B., Suciu, R.M., Roper, J., Luopajärvi, K., Markelin, E., Gopalakrishnan, S., et al. (2019). Notum produced by Paneth cells attenuates regeneration of aged intestinal epithelium. Nature *571*, 398–402. https://doi.org/10.1038/s41586-019-1383-0.

Perri, E.R., Thomas, C.J., Parakh, S., Spencer, D.M., and Atkin, J.D. (2016). The unfolded protein response and the role of protein disulfide isomerase in neurodegeneration. Front. Cell Dev. Biol. *3*, 1–17. https://doi.org/10.3389/fcell.2015.00080.

Reya, T., and Clevers, H. (2005). Wnt signalling in stem cells and cancer. Nature *434*, 843–850. https://doi.org/10.1038/nature03319.

Rutkevich, L.A., Cohen-Doyle, M.F., Brockmeier, U., and Williams, D.B. (2010). Functional relationship between protein disulfide isomerase family members during the oxidative folding of human secretory proteins. Mol. Biol. Cell *21*, 3093–3105. https://doi.org/10.1091/mbc.e10-04-0356.

Shao, L.W., Niu, R., and Liu, Y. (2016). Neuropeptide signals cell non-autonomous mitochondrial unfolded protein response. Cell Res. *26*, 1182–1196. https://doi.org/10.1038/cr.2016.118.

Shao, L.W., Peng, Q., Dong, M., Gao, K., Li, Y., Li, Y., Li, C.Y., and Liu, Y. (2020). Histone deacetylase HDA-1 modulates mitochondrial stress response and longevity. Nat. Commun. *11*, 4639–4712. https://doi.org/10.1038/s41467-020-18501-w.

Shpilka, T., and Haynes, C.M. (2018). The mitochondrial UPR: mechanisms, physiological functions and implications in ageing. Nat. Rev. Mol. Cell Biol. *19*, 109–120. https://doi.org/10.1038/nrm.2017.110.

Sugioka, K., Mizumoto, K., and Sawa, H. (2011). Wnt regulates spindle asymmetry to generate asymmetric nuclear β-catenin in *C. elegans*. Cell *146*, 942–954. https://doi.org/10.1016/j.cell.2011.07.043.

Suomalainen, A., Elo, J.M., Pietiläinen, K.H., Hakonen, A.H., Sevastianova, K., Korpela, M., Isohanni, P., Marjavaara, S.K., Tyni, T., Kiuru-Enari, S., et al. (2011). FGF-21 as a biomarker for muscle-manifesting mitochondrial respiratory chain deficiencies: a diagnostic study. Lancet Neurol. *10*, 806–818. https://doi.org/10.1016/s1474-4422(11)70155-7.

Taylor, R.C., and Dillin, A. (2013). XBP-1 is a cell-nonautonomous regulator of stress resistance and longevity. Cell *153*, 1435–1447. https://doi.org/10.1016/j.cell.2013.05.042.

Tian, Y., Garcia, G., Bian, Q., Steffen, K.K., Joe, L., Wolff, S., Meyer, B.J., and Dillin, A. (2016). Mitochondrial stress induces chromatin reorganization to promote longevity and UPR^{mt}. Cell *165*, 1197–1208. https://doi.org/10.1016/j.cell.2016.04.011.

Torpe, N., Gopal, S., Baltaci, O., Rella, L., Handley, A., Korswagen, H.C., and Pocock, R. (2019). A protein disulfide isomerase controls neuronal migration through regulation of Wnt secretion. Cell Rep. *26*, 3183–3190.e5. https://doi.org/10.1016/j.celrep.2019.02.072.

Uehara, T., Nakamura, T., Yao, D., Shi, Z.Q., Gu, Z., Ma, Y., Masliah, E., Nomura, Y., and Lipton, S.A. (2006). S-Nitrosylated protein-disulphide isomerase links protein misfolding to neurodegeneration. Nature *441*, 513–517. https://doi.org/10.1038/nature04782.

Ushioda, R., Hoseki, J., Araki, K., Jansen, G., Thomas, D.Y., and Nagata, K. (2008). ERdj5 is required as a disulfide reductase for degradation of misfolded proteins in the ER. Science *321*, 569–572. https://doi.org/10.1126/science.1159293.

Waaijers, S., Portegijs, V., Kerver, J., Lemmens, B.B.L.G., Tijsterman, M., van den Heuvel, S., and Boxem, M. (2013). CRISPR/Cas9-targeted mutagenesis in *Caenorhabditis elegans*. Genetics *195*, 1187–1191. https://doi.org/10.1534/genetics.113.156299.

Whangbo, J., and Kenyon, C. (1999). A Wnt signaling system that specifies two patterns of cell migration in *C. elegans*. Mol. Cell *4*, 851–858. https://doi.org/10.1016/s1097-2765(00)80394-9.

Willert, K., and Nusse, R. (2012). Wnt proteins. Cold Spring Harb. Perspect. Biol. *4*, a007864–14. https://doi.org/10.1101/cshperspect.a007864.

Wodarz, A., and Nusse, R. (1998). Mechanisms of Wnt signaling in development. Annu. Rev. Cell Dev. Biol. *14*, 59–88. https://doi.org/10.1146/annurev.cellbio.14.1.59.

Wolkow, C.A., Kimura, K.D., Lee, M.S., and Ruvkun, G. (2000). Regulation of *C. elegans* life-span by insulinlike signaling in the nervous system. Science *290*, 147–150. https://doi.org/10.1126/science.290.5489.147.

Yoneda, T., Benedetti, C., Urano, F., Clark, S.G., Harding, H.P., and Ron, D. (2004). Compartment-specific perturbation of protein handling activates genes encoding mitochondrial chaperones. J. Cell Sci. *117*, 4055–4066. https://doi.org/10.1242/jcs.01275.

Yoo, J.K., Choi, S.J., and Kim, J.K. (2013). Expression profiles of subtracted mRNAs during cellular senescence in human mesenchymal stem cells derived from bone marrow. Exp. Gerontol. *48*, 464–471. https://doi.org/10.1016/j.exger.2013.02.022.

Zhang, J., Liu, J., Norris, A., Grant, B.D., and Wang, X. (2018a). A novel requirement for ubiquitin-conjugating enzyme UBC-13 in retrograde recycling of MIG-14/Wntless and Wnt signaling. Mol. Biol. Cell *29*, 2098–2112. https://doi.org/10.1091/mbc.e17-11-0639.

Zhang, Q., and Tian, Y. (2022). Molecular insights into the transgenerational inheritance of stress memory. J. Genet. Genomics *49*, 89–95. https://doi.org/10.1016/j.jgg.2021.11.015.

Zhang, Q., Wang, Z., Zhang, W., Wen, Q., Li, X., Zhou, J., Wu, X., Guo, Y., Liu, Y., Wei, C., et al. (2021). The memory of neuronal mitochondrial stress is inherited transgenerationally via elevated mitochondrial DNA levels. Nat. Cell Biol. *23*, 870–880. https://doi.org/10.1038/s41556-021-00724-8.

Zhang, Q., Wu, X., Chen, P., Liu, L., Xin, N., Tian, Y., and Dillin, A. (2018b). The mitochondrial unfolded protein response is mediated cell-non-autonomously by retromer-dependent Wnt signaling. Cell *174*, 870–883.e17. https://doi.org/10.1016/j.cell.2018.06.029.

Zhou, J., Wu, Y., Wang, L., Rauova, L., Hayes, V.M., Poncz, M., and Essex, D.W. (2015). The C-terminal CGHC motif of protein disulfide isomerase supports thrombosis. J. Clin. Invest. *125*, 4391–4406. https://doi.org/10.1172/jci80319.

Zhou, X., Li, G., Kaplan, A., Gaschler, M.M., Zhang, X., Hou, Z., Jiang, M., Zott, R., Cremers, S., Stockwell, B.R., and Duan, W. (2018). Small molecule modulator of protein disulfide isomerase attenuates mutant huntingtin toxicity and inhibits endoplasmic reticulum stress in a mouse model of Huntington's disease. Hum. Mol. Genet. *27*, 1545–1555. https://doi.org/10.1093/hmg/ddy061.

Zhu, D., Li, X., and Tian, Y. (2022). Mitochondrial-to-nuclear communication in aging: an epigenetic perspective. Trends Biochem. Sci. Published online April *6*, 2022. https://doi.org/10.1016/j.tibs.2022.03.008.

Zhu, D., Wu, X., Zhou, J., Li, X., Huang, X., Li, J., Wu, J., Bian, Q., Wang, Y., and Tian, Y. (2020). NuRD mediates mitochondrial stress–induced longevity via chromatin remodeling in response to acetyl-CoA level. Sci. Adv. *6*, 1–13. https://doi.org/10.1126/sciadv.abb2529.

STAR★METHODS

KEY RESOURCES TABLE

REAGENT or RESOURCE	SOURCE	IDENTIFIER
Antibodies		
Mouse monoclonal anti-GFP (B-2)	Santa Cruz Biotechnology	Cat#sc-9996; RRID: AB_627695
Mouse monoclonal anti-Tubulin (B-5-1-2)	Sigma	Cat#T6074; RRID: AB_477582
Rabbit polyclonal anti-RFP	Rockland	Cat#600-401-379s; RRID: AB_11182807
HRP-Goat anti-mouse IgG	EarthOx	Cat#E030110; RRID: AB_2572419
HRP-Goat anti-Rabbit IgG	EASYBIO	Cat#BE0101
Bacterial and virus strains		
OP50	CGC	N/A
HT115	CGC	N/A
DH5α	Tiangen	Cat#CB101
Chemicals, peptides, and recombinant proteins		
Agarose	Life Technology	Cat#202007
GeneGreen	Tiangen	Cat#RT210
Ethylenediamine tetraacetic acid	Sigma	Cat#E9884
Trizma base	Sigma	Cat#V900483
Sodium chloride	Sigma	Cat#V900058
Bacto Agar	BD	Cat#214010
Bacto Peptone	BD	Cat#211677
Cholesterol	Sigma	Cat#C8667
Calcium chloride dehydrate	Sigma	Cat#C7902
Magnesium sulfate heptahydrate	Sigma	Cat#M1880
Potassium phosphate monobasic	Sigma	Cat#V900041
Potassium phosphate dibasic	Sigma	Cat#V900050
Sodium phosphate dibasic	Sigma	Cat#V900061
Isopropyl beta-D-thiogalactoside	Sigma	Cat#V900917
Carbenicillin Na_2	INALCO	Cat#1758-9317
TRYPTONE	OXOID	Cat#CM0129
YEAST EXTRACT	OXOID	Cat#LP0021
Potassium chloride	Sigma	Cat#V900068
Glycine	Amresco	Cat#0167
Tween 20	Sigma	Cat#P1379
TEMED	Sigma	Cat#T22500
Ammonium persulfate	Sigma	Cat#V900883
Sodium dodecyl sulfate	Sigma	Cat#V900859
TBT transfer buffer	BIO-RAD	Cat#10026938
TRIzol	Invitrogen	Cat#15596026
Sodium acetate buffer solution	Sigma	Cat#S7899
FUDR	Aladdin	Cat#F110732
Tunicamycin	Abcam	Cat#ab120296
Carbonyl cyanide 3-chlorophenylhydrazone	Sigma	Cat# C2759
Paraquat	Macklin	Cat#M813276
LDS Sample Buffer, Non-Reducing (4×)	Pierce	Cat#84788
NUPAGE Sample Reducing Agent	Thermo Scientific	Cat#NP0009

(*Continued on next page*)

Continued

REAGENT or RESOURCE	SOURCE	IDENTIFIER
Critical commercial assays		
TGX FastCast Acrylamide Kit, 10%	BIO-RAD	Cat#1610172
Tanon High-sig ECL Western Blotting Substrate	Tanon	Cat#180-501
M-MLV Reverse Transcriptase	Invitrogen	Cat#28025013
KOD-Plus-Neo	Toyobo	Cat#KOD-401
RQ1 RNase-Free DNase	Promega	Cat#M6101
RNasin Ribonuclease Inhibitor	Promega	Cat#N2111
iTaq Universal SYBR Green Supermix	BIO-RAD	Cat#1725121
QIAprep Spin Miniprep Kit	QIAGEN	Cat#27104
2 × Rapid Taq Master Mix	Vazyme	Cat#P222-03
KOD-Plus-Mutagenesis Kit	Toyobo	Cat#SMK-101
One Step Cloning Kit	Vazyme	Cat#C112
SYBR Green Premix Pro Taq HS qPCR Kit	AG	Cat#AG11701
PrimeScript RT reagent Kit with gDNA Eraser	Toyobo	Cat#FSQ-301
Experimental models: Organisms/strains		
C. elegans: Bristol (N2) strain as wild-type (WT)	CGC	N2
C. elegans: SJ4100 (zcIs13[*hsp-6p*::*gfp*] V)	CGC	WormBase ID: SJ4100
C. elegans: SJ4005 (zcIs4[*hsp-4p*::*gfp*] V)	CGC	WormBase ID: SJ4005
C. elegans: CL2070 (dvIs70[*hsp-16.2p*::*gfp* + *rol-6(su1006)*])	CGC	WormBase ID: CL2070
C. elegans: SJ4197 (zcIs39[*dve-1p*::*dve-1*::*gfp*])	CGC	WormBase ID: SJ4197
C. elegans: AM101 (rmIs110[*rgef-1p*::*Q40*::*yfp*]	CGC	WormBase ID: AM101
C. elegans: *hrd-1(tm1743)* V	National Bioresource Project, Tokyo, Japan	WormBase ID: WBVar00250708
C. elegans: *xbp-1(tm2482)* III	National Bioresource Project, Tokyo, Japan	WormBase ID: WBVar00251364
C. elegans: MT1215 (*egl-20(n585)* IV)	CGC	WormBase ID: MT1215
C. elegans: VC586 (*pdi-1(gk271)* III)	CGC	WormBase ID: VC586
C. elegans: TP66 (*pdi-3(ka1)* III)	CGC	WormBase ID: TP66
C. elegans: VS30 (hjSi158 [*vha-6p*::*SEL-1(1–79)*::*mCherry*::*HDEL*::*let-858* 3′UTR] I)	CGC	WormBase ID: VS30
C. elegans: LTY1537 (hjSi158 *[vha-6p*::*SEL-1(1–79)*::*mCherry*::*HDEL*::*let-858 3′UTR*] I; syb2068[*pdi-6*::*gfp*] X)	This paper	N/A
C. elegans: CF1045 (muIs49[*unc-22(+)* + *egl-20p*::*egl-20*::*gfp*])	CGC	WormBase ID: CF1045
C. elegans: LTY1174 (ythIs35[*pdi-6p*::*pdi-6*::*mCherry* + *rol-6(su1006)*]; muIs49 *[unc-22(+) egl-20p*::*egl-20*::*gfp*])	This paper	N/A
C. elegans: LTY1831 (ythEx319[*pdi-6p*::*pdi-6(trapping mutant)*::*mCherry*::*HA* + *rol-6(su1006)*]; muIs49 *[unc-22(+) egl-20p*::*egl-20*::*gfp*])	This paper	N/A
C. elegans: LTY2002 (ythEx357[*pdi-6p*::*pdi-6(OO-OO)*::*mCherry*::*HA* + *rol-6(su1006)*]; muIs49 *[unc-22(+) egl-20p*::*egl-20*::*gfp*])	This paper	N/A
C. elegans: LTY2260 (ythEx357[*pdi-6p*::*pdi-6(OO-OO)*::*mCherry*::*HA* + *rol-6(su1006)*])	This paper	N/A

(*Continued on next page*)

Continued

REAGENT or RESOURCE	SOURCE	IDENTIFIER
C. elegans: LTY1833 (ythEx357[*pdi-6p*::*pdi-6(trapping mutant)*::*mCherry*::*HA* + *rol-6(su1006)*])	This paper	N/A
C. elegans: LTY1433 (ythIs34[*pdi-6p*::*pdi-6*::*mCherry* + *rol-6(su1006)*])	This paper	N/A
C. elegans: LTY1434 (ythIs35[*pdi-6p*::*pdi-6*::*mCherry* + *rol-6(su1006)*])	This paper	N/A
C. elegans: SJZ204 (foxSi37[*ges-1p*::*tomm-20*::*mKate2*::*HA*::*tbb-2* 3′ UTR] I)	CGC	WormBase ID: SJZ204
C. elegans: XW6096 (qxIs352[*ced-1p*::*laat-1*::*mCherry*])	Miao et al., 2020	N/A
C. elegans: LTY2562 (*syb2068*[*pdi-6*::*gfp*] X; qxIs352[*ced-1p*::*laat-1*::*mCherry*])	This paper	N/A
C. elegans: GR1333 (yzIs71[*tph-1p*::*gfp* + *rol-6(su1006)*] V)	CGC	WormBase ID: GR1333
C. elegans: LTY770 (*rrf-3(pk1426)* II; yzIs71 [*tph-1p*::*gfp* + *rol-6(su1006)*] V)	This paper	N/A
C. elegans: LTY718 (*egl-20(n585)* IV; yzIs71 [*tph-1p*::*gfp* + *rol-6(su1006)*] V)	This paper	N/A
C. elegans: LTY764 (*pdi-1(gk271)* III; yzIs71 [*tph-1p*::*gfp* + *rol-6(su1006)*] V)	This paper	N/A
C. elegans: LTY2352 (*pdi-3(ka1)* III; yzIs71 [*tph-1p*::*gfp* + *rol-6(su1006)*] V)	This paper	N/A
C. elegans: LTY2558 (*pdi-6(yth109)* III; yzIs71[*tph-1p*::*gfp* + *rol-6(su1006)*] V)	This paper	N/A
C. elegans: LTY2559 (*pdi-6(yth112)* III; yzIs71[*tph-1p*::*gfp* + *rol-6(su1006)*] V)	This paper	N/A
C. elegans: CF702 (muIs32[*mec-7p*::*gfp* + *lin-15(+)*])	CGC	WormBase ID: CF702
C. elegans: LTY1442 (muIs32[*mec-7p*::*gfp* + *lin-15(+)*].II; *egl-20(n585)* IV)	This paper	N/A
C. elegans: LTY2349 (muIs32[*mec-7p*::*gfp* + *lin-15(+)*].II; *rrf-3(pk1426)* II)	This paper	N/A
C. elegans: LTY2350 (muIs32[*mec-7p*::*gfp* + *lin-15(+)*].II; *pdi-1(gk271)* III)	This paper	N/A
C. elegans: LTY2351 (muIs32[*mec-7p*::*gfp* + *lin-15(+)*].II; *pdi-3(ka1)* III)	This paper	N/A
C. elegans: LTY2560 (muIs32[*mec-7p*::*gfp* + *lin-15(+)*].II; *pdi-6(yth109)* X)	This paper	N/A
C. elegans: LTY2561 (muIs32[*mec-7p*::*gfp* + *lin-15(+)*].II; *pdi-6(yth112)* X)	This paper	N/A
C. elegans: AGD1079 (*sid-1(qt9)*; uthIs375 [*unc-119p*::*cco-1HP* + *rol-6(su1006)]*	Durieux et al., 2011	N/A
C. elegans: PHX2068 (*syb2068*[*pdi-6*::*gfp*] X)	Sunybiotech	N/A
C. elegans: VC3201 (*atfs-1*(*gk3094*) V)	CGC	WormBase ID: VC3201
C. elegans: LTY39 (ythIs3[*rgef-1p*::*egl-20* + *myo-2p*::*tdTomato*] IV; zcIs39[*dve-1p*::*dve-1*::*gfp*] II)	Zhang et al., 2018b	N/A
C. elegans: LTY693 (*pdi-6(yth16)* X)	This paper	N/A
C. elegans: LTY2445 (*pdi-6(yth112)* X)	This paper	N/A
C. elegans: LTY297 (*pdi-6(yth16)* X; ythIs3 [*rgef-1p*::*egl-20* + *myo-2p*::*tdTomato*] IV; zcIs39[*dve-1p*::*dve-1*::*gfp*] II)	This paper	N/A

(*Continued on next page*)

Continued

REAGENT or RESOURCE	SOURCE	IDENTIFIER
C. elegans: LTY2539 (*pdi-6(yth112)* X; ythIs3[*rgef-1p::egl-20* + *myo-2p::tdTomato*] IV; zcIs39[*dve-1p::dve-1::gfp*] II)	This paper	N/A
C. elegans: LTY2542 (*pdi-6(yth112)* X; rmIs110[*rgef-1p::Q40::yfp*]; zcIs13[*hsp-6p::gfp*] V)	This paper	N/A
C. elegans: AGD785 (rmIs110[*rgef-1p::Q40::yfp*] X; zcIs13[*hsp-6p::gfp*] V)	Berendzen et al., 2016	N/A
C. elegans: AGD1075 (*sid-1(qt9)* V; zcIs13 [*hsp-6p::gfp*] V; uthIs375[*unc-119p::cco-1* HP + *rol-6(su1006)*])	Durieux et al., 2011	N/A
C. elegans: LTY2547 (*pdi-6(yth112)* X; *sid-1(qt9)* V; zcIs13[*hsp-6p::gfp*] V; uthIs375 [*unc-119p::cco-1* HP + *rol-6(su1006)*])	This paper	N/A
C. elegans: LTY2437 (*pdi-6(yth104)* X)	This paper	N/A
C. elegans: LTY2442 (*pdi-6(yth109)* X)	This paper	N/A
C. elegans: LTY2537 (*pdi-6(yth104)* X; ythIs3[*rgef-1p::egl-20* + *myo-2p::tdTomato*] IV; zcIs39[*dve-1p::dve-1::gfp*] II)	This paper	N/A
C. elegans: LTY2538 (*pdi-6(yth109)* X; ythIs3[*rgef-1p::egl-20* + *myo-2p::tdTomato*] IV; zcIs39[*dve-1p::dve-1::gfp*] II)	This paper	N/A
C. elegans: LTY43 (ythIs3[*rgef-1p::egl-20* + *myo-2p::tdTomato*]; zcIs13[*hsp-6p::gfp*] V)	Zhang et al., 2018b	N/A
C. elegans: LTY2540 (*pdi-6(yth104)* X; ythIs3[*rgef-1p::egl-20* + *myo-2p::tdTomato*] IV; zcIs13[*hsp-6p::gfp*] V)	This paper	N/A
C. elegans: LTY2541 (*pdi-6(yth109)* X; ythIs3[*rgef-1p::egl-20* + *myo-2p::tdTomato*] IV; zcIs13[*hsp-6p::gfp*] V)	This paper	N/A
C. elegans: LTY2542 (*pdi-6(yth112)* X; ythIs3[*rgef-1p::egl-20* + *myo-2p::tdTomato*] IV; zcIs13[*hsp-6p::gfp*] V)	This paper	N/A
C. elegans: AGD1366 (rmIs110[*rgef-1p::Q40::yfp*]; zcIs39[*dve-1p::dve-1::gfp*] II)	Berendzen et al., 2016	N/A
C. elegans: LTY2543 (*pdi-6(yth104)* X; rmIs110[*rgef-1p::Q40::yfp*] X; zcIs39[*dve-1p::dve-1::gfp*] II)	This paper	N/A
C. elegans: LTY2544 (*pdi-6(yth109)* X; rmIs110[*rgef-1p::Q40::yfp*] X; zcIs39[*dve-1p::dve-1::gfp*] II)	This paper	N/A
C. elegans: LTY2545 (*pdi-6(yth112)* X; rmIs110[*rgef-1p::Q40::yfp*] X; zcIs39[*dve-1p::dve-1::gfp*] II)	This paper	N/A
C. elegans: LTY2438 (*pdi-6(yth105)*/+ X)	This paper	N/A
C. elegans: LTY2439 (*pdi-6(yth106)*/+ X)	This paper	N/A
C. elegans: LTY2548 (*pdi-6(yth112)* X; rmIs110[*rgef-1p::Q40::yfp*]; zcIs13[*hsp-6p::gfp*] V; ythIs35 [*pdi-6p::pdi-6::mCherry* + *rol-6(su1006)*])	This paper	N/A
C. elegans: LTY2549 (*pdi-6(yth112)* X; rmIs110[*rgef-1p::Q40::yfp*]; zcIs13[*hsp-6p::gfp*] V; ythEx182 [*rgef-1p::pdi-6* + *rol-6(su1006)*])	This paper	N/A

(*Continued on next page*)

Continued

REAGENT or RESOURCE	SOURCE	IDENTIFIER
C. elegans: LTY2550 (*pdi-6(yth112)* X; rmIs110[*rgef-1p::Q40::yfp*]; zcIs13[*hsp-6p::gfp*] V; ythEx186 [*gly-19p::pdi-6 + rol-6(su1006)*])	This paper	N/A
C. elegans: LTY2551 (*pdi-6(yth112)* X; rmIs110[*rgef-1p::Q40::yfp*]; zcIs13[*hsp-6p::gfp*] V; ythEx156 [*egl-20p::pdi-6 + rol-6(su1006)*])	This paper	N/A
C. elegans: LTY2025 (rmIs110[*rgef-1p::Q40::yfp*]; *syb2068[pdi-6::gfp]* X)	This paper	N/A
C. elegans: LTY2026 (*sid-1(qt9)* V; uthIs375 [*unc-119p::cco-1* HP + *rol-6(su1006)*]; *syb2068[pdi-6::gfp]* X)	This paper	N/A
C. elegans: AGD928 (uthIs270[*rab-3p::xbp-1s + myo-2p::tdTomato*]; zcIs4[*hsp-4p::gfp*] V)	Taylor and Dillin, 2013	N/A
C. elegans: AGD1199 (uthIs368[*rab-3p::hsf-1 + myo-2p::tdTomato*]; muIs84[sod-3p::gfp])	Douglas et al., 2015	N/A
C. elegans: LTY1231 (*pdi-6(yth112)* X; uthIs270[*rab-3p::xbp-1s + myo-2p::tdTomato*]; zcIs4[*hsp-4p::gfp*] V)	This paper	N/A
C. elegans: LTY2552 (*pdi-6(yth112)* X; zcIs13[*hsp-6p::gfp*] V)	This paper	N/A
C. elegans: LTY2553 (*pdi-6(yth112)* X; zcIs4 [*hsp-4p::gfp*] V))	This paper	N/A
C. elegans: LTY2554 (*pdi-6(yth112)* X; dvIs70[*hsp-16.2p::gfp + rol-6(su1006)*])	This paper	N/A
C. elegans: LTY59 (ythIs8[*egl-20p::egl-20::mCherry + rol-6(su1006)*])	Zhang et al., 2018b	N/A
C. elegans: LTY2555 (*pdi-6(yth112)* X; ythIs8[*egl-20p::egl-20::mCherry + rol-6(su1006)*])	This paper	N/A
C. elegans: LTY1830 (*syb2068[pdi-6::gfp]* X; ythIs8[*egl-20p::egl-20::mCherry + rol-6(su1006)*])	This paper	N/A
C. elegans: LTY2353 (*hrd-1(tm1743)* V; ythIs8[*egl-20p::egl-20::mCherry + rol-6(su1006)*])	This paper	N/A
C. elegans: LTY2556 (*hrd-1(tm1743)* V; *pdi-6(yth112)* X; ythIs8[*egl-20p::egl-20::mCherry + rol-6(su1006)*])	This paper	N/A
C. elegans: LTY2605 (ythSi26[*pdi-6p::pdi-6(trapping murant::gfp*]; ythIs8[*egl-20p::egl-20::mCherry + rol-6(su1006)*])	This paper	N/A
C. elegans: LTY760 (*pdi-1(gk271)* III; ythIs3 [*rgef-1p::egl-20 + myo-2p::tdTomato*] IV; zcIs13[*hsp-6p::gfp*] V)	This paper	N/A
C. elegans: LTY1950 (*pdi-3(ka1)* III; ythIs3 [*rgef-1p::egl-20 + myo-2p::tdTomato*] IV; zcIs13[*hsp-6p::gfp*] V)	This paper	N/A
C. elegans: LTY56 (ythIs6[*egl-20p::mCherry + rol-6(su1006)*])	Zhang et al., 2018b	N/A

(*Continued on next page*)

Continued

REAGENT or RESOURCE	SOURCE	IDENTIFIER
C. elegans: LTY707 (ythIs6[*egl-20p::mCherry + rol-6(su1006)*]; *pdi-6(yth112)* X)	This paper	N/A
C. elegans: qxIs618[*egl-20p::mig-14::gfp*]	Zhang et al., 2018a	N/A
C. elegans: LTY2554 (*pdi-6(yth112)* X; qxIs618[*egl-20p::mig-14::gfp*])	This paper	N/A
C. elegans: LTY2606 (*pdi-6(yth112)* X; rmIs110[*rgef-1p::Q40::yfp*] X; zcIs13[*hsp-6p:: gfp*] V; ythEx301[*pdi-6p::pdi-6(Δa)::mCherry::HA + rol-6(su1006)*])	This paper	N/A
C. elegans: LTY2607 (*pdi-6(yth112)* X; rmIs110[*rgef-1p::Q40::yfp*] X; zcIs13[*hsp-6p:: gfp*] V; ythEx304[*pdi-6p::pdi-6(Δa')::mCherry::HA + rol-6(su1006)*])	This paper	N/A
C. elegans: LTY2608 (*pdi-6(yth112)* X; rmIs110[*rgef-1p::Q40::yfp*] X; zcIs13[*hsp-6p:: gfp*] V; ythEx307[*pdi-6p::pdi-6(Δb)::mCherry::HA + rol-6(su1006)*])	This paper	N/A
C. elegans: LTY2603 (*pdi-6(yth112)* X; rmIs110[*rgef-1p::Q40::yfp*] X; zcIs13[*hsp-6p:: gfp*] V; ythEx316[*pdi-6p::pdi-6(OO-OO)::mCherry::HA + rol-6(su1006)*])	This paper	N/A
C. elegans: LTY1225 (ythIs35[*pdi-6p::pdi-6::mCherry + rol-6(su1006)*]; zcIs13[*hsp-6p:: gfp*] V)	This paper	N/A
C. elegans: LTY2671 (ythEx182[*rgef-1p::pdi-6 + rol-6(su1006)*]; zcIs13[*hsp-6p:: gfp*] V)	This paper	N/A
C. elegans: LTY2679 (ythEx182[*rgef-1p::pdi-6 + rol-6(su1006)*]; *egl-20(n585)* IV)	This paper	N/A
C. elegans: LTY2563 (*hrd-1(tm1743)* V; *syb2068[pdi-6::gfp]* X)	This paper	N/A
C. elegans: LTY2265 (*egl-20(n585)* IV; ythIs35[*pdi-6p::pdi-6::mCherry + rol-6(su1006)*])	This paper	N/A
C. elegans: LTY2266 (*atfs-1(gk3094)* V; ythIs35[*pdi-6p::pdi-6::mCherry + rol-6(su1006)*])	This paper	N/A
C. elegans: LTY2267 (*xbp-1(tm2482)* III; ythIs35[*pdi-6p::pdi-6::mCherry + rol-6(su1006)*])	This paper	N/A
C. elegans: LTY2255 (ythEx182[*rgef-1p::pdi-6 + rol-6(su1006)*])	This paper	N/A
C. elegans: LTY2675 (ythEx182[*rgef-1p::pdi-6 + rol-6(su1006)*]; zcIs13[*hsp-6p:: gfp*] V; *egl-20(n585)* IV)	This paper	N/A
C. elegans: LTY2679 (ythEx182[*rgef-1p::pdi-6 + rol-6(su1006)*]; *egl-20(n585)* IV)	This paper	N/A
C. elegans: LTY2683 (ythEx182[*rgef-1p::pdi-6 + rol-6(su1006)*]; *atfs-1(gk3094)* V)	This paper	N/A
C. elegans: LTY1283 (ythEx186[*gly-19p::pdi-6 + rol-6(su1006)*])	This paper	N/A
C. elegans: LTY2257 (ythEx200[*lin-26p::pdi-6 + rol-6(su1006)*])	This paper	N/A

(*Continued on next page*)

Continued		
REAGENT or RESOURCE	SOURCE	IDENTIFIER
C. elegans: LTY2258 (ythEx200[*myo-3p::pdi-6 + rol-6(su1006)*])	This paper	N/A
Oligonucleotides		
Primers	See Table S2 for primers used in this paper	N/A
Recombinant DNA		
pdi-6p::pdi-6::mCherry	This paper	N/A
pdi-6p::pdi-6(Δa)::mCherry::HA	This paper	N/A
pdi-6p::pdi-6(Δa')::mCherry::HA	This paper	N/A
pdi-6p::pdi-6(Δb)::mCherry::HA	This paper	N/A
pdi-6p::pdi-6(OO-OO)::mCherry::HA	This paper	N/A
pdi-6p::pdi-6(trapping mutant)::mCherry::HA	This paper	N/A
rgef-1p::pdi-6	This paper	N/A
gly-19p::pdi-6	This paper	N/A
egl-20p::pdi-6	This paper	N/A
lin-26p::pdi-6	This paper	N/A
myo-3p::pdi-6	This paper	N/A
Software and algorithms		
GraphPad Prism 6	GraphPad Software	https://www.graphpad.com/scientificsoftware/prism/
Excel 2017	Microsoft	https://products.office.com/en-us/excel
ImageJ 1.48v	Wayne Rasband (NIH)	https://imagej.nih.gov/ij/
Zen	Zeiss	https://www.zeiss.com/microscopy/us/products/microscope-software/zen.html

RESOURCE AVAILABILITY

Lead contact

Further information and requests for resources and reagents should be directed to and will be fulfilled by the lead contact, Ye Tian (ytian@genetics.ac.cn).

Materials availability

All unique/stable reagents generated in this study are available from the lead contact with a completed Material Transfer Agreement.

Data and code availability

- Original western blot images and microscopy data reported in this paper will be shared by the lead contact upon request.
- This paper does not report the original code.
- Any additional information required to reanalyze the data reported in this paper is available from the lead contact upon request.

EXPERIMENTAL MODEL AND SUBJECT DETAILS

Caenorhabditis elegans maintenance

Studies were undertaken with *C. elegans* hermaphrodites. Nematodes were maintained and experimentally examined at 20°C on standard nematode growth medium (NGM) agar plates seeded with *Escherichia coli* OP50, unless otherwise indicated. Strains used or generated are reported in the key resources table.

METHOD DETAILS

EMS mutagenesis screen

Approximately 100 L4 worms were collected, washed with M9 buffer three times and suspended in 3 mL M9 buffer. 20 μL EMS (Ethyl Methane sulfonate, Sigma #M-0880) was added into 1mL M9 buffer. The 3 mL M9 buffer containing worms were mixed with the 1mL EMS solution, making the final concentration of EMS to 47 mM and incubated at 20°C on a spinning wheel for 4 h. Then, worms were

washed with M9 buffer and transferred to NGM plates. Healthy looking late L4 animals were picked off to be P0. F1 progeny were then allowed to be self-fertilized, and F2 animals were screened for the suppressed *dve-1p::dve-1::gfp* phenotype.

Gene mapping

Mutants identified from the EMS mutagenesis were outcrossed with the wild-type *rgef-1p::egl-20; dve-1p::dve-1::gfp* animals at least three times. Mutants were crossed with wild-type *rgef-1p::egl-20; dve-1p::dve-1::gfp* animals and the F2 animals with *rgef-1p::egl-20* and suppressed *dve-1p::dve-1::gfp* were selected. After being outcrossed, the mutants were subjected to the whole-genome sequencing. Meanwhile, the mutants were outcrossed with animals expressing *rgef-1p::egl-20; dve-1p::dve-1::gfp* in CB4856 (Hawaiian) background and F2 animals with suppressed *dve-1p::dve-1::gfp* expression were subjected for single nucleotide polymorphism (SNP) mapping following published protocols (Davis et al., 2005). *yth16* was mapped to the X chromosome and the whole-genome sequencing results indicated that there are SNPs in exons of four genes located on the X chromosome: *pks-1*, *pdi-6*, *C44C10.10,* and *B0198.2*. Candidate RNAi screen against these four genes was performed.

Generation of different alleles of *pdi-6* mutants

The *pdi-6* mutant worms were created using CRISPR/Cas9 technology in accordance with published protocols (Waaijers et al., 2013). *pdi-6(yth105)*, *pdi-6(yth106)*, and *pdi-6(yth112)* were generated using the guide RNA sequence GGCGACGACAGT ATGAACAG and TCTGGATCTGGAAAGCGTGG. *pdi-6(yth104)* and *pdi-6(yth109)* were generated using the guide RNA sequence TGATGTCGTCGAGCTGACCG and ATGACTCAACATCAATCCGT.

RNAi feeding

Age synchronized worms were bleached with bleaching buffer (1.5% NaClO; 0.65M KOH) and grown from hatch on *Escherichia coli* HT115 strains containing an empty vector control or double-stranded RNA. RNAi strains were purchased from the Vidal library if present, or the Ahringer library if they were absent from the Vidal library.

Co-immunoprecipitation

Worms in mixed stages grown on plates were collected and washed in M9 buffer. After washing, the animals were re-suspended in 0.5 volumes of extraction buffer (50 mM Tris-HCL, pH 7.4; 150 mM NaCl; 10% glycerol; 0.1% NP-40 and protease inhibitors). For non-reducing conditions, the animals were re-suspended in extraction buffer with 50mM NEM. The suspension was then dripped into liquid N2, and the resulting balls were ground using mortar and pestle. The homogenized worm tissue was re-suspended with 2 volumes of extraction buffer, and lysed at 4°C for 30 min, the insoluble materials were then removed by centrifugation at 13000 rpm, 4°C.

For Co-immunoprecipitation, 2 mL lysates were mixed with GFP-trap Agarose (Chromotek) (20 μL) for 4 h. Immunoprecipitates were washed four times with wash buffer (50 mM Tris-HCL, pH 7.4; 250 mM NaCl; 10% glycerol and protease inhibitors). Samples were then subjected to Western blot analysis.

Heat shock assay

Synchronized day 1 adult worms of different genetic backgrounds were incubated in 34°C for 20 min. After 6 h recovery, worms were imaged using a Leica M165 FC dissecting microscope.

Transgenic strain construction

The *pdi-6* 2.1 kb promoter and *pdi-6* coding sequence (1899 bp) without stop codon, which contains a flexible linker (GASGASGAS) and a mCherry tag, were used to generate *pdi-6p::pdi-6::mCherry*. To replace *pdi-6* promoter, the *rgef-1*, *gly-19*, *lin-26*, *myo-3* and *egl-20* promoter was cloned in place of the *pdi-6* promoter in the *pdi-6p::pdi-6::unc-54 UTR* plasmid. To replace PDI-6 with PDI-6(trapping mutant), PDI-6(OO-OO), PDI-6(Δa), PDI-6(Δa′) and PDI-6(Δb), we use KOD-plus-Mutagenesis Kit to generate PDI-6[OO-OO (C37S, C39S; C144S, C146S)], PDI-6[trapping mutant (C39A; C146A)], PDI-6[Δa (Δ25-127 amino acid)], PDI-6[Δa′ (Δ165-269 amino acid)] and PDI-6[Δb (Δ278-407 amino acid)] plasmid. mCherry was from pBR322 backbone and One Step Cloning Kit (Vazyme) was used for cloning.

Transgenic strains were generated by microinjecting target constructs (1–40 ng/μL) mixed with a pRF4(*rol-6*) (60 ng/μL) co-injection maker. Integrated lines were generated using UV irradiation and outcrossed six times with wild-type animals.

Examination of QL.d and HSN migration

The final position of left Q cell descendants (QL.d) and HSNs was determined using Nomarski optics in young adult animals (Torpe et al., 2019). The position of QL.d and HSNs was determined with respect to the seam cell daughters V1.a to V6.p. For *pdi-2* and *c14b9.2* RNAi assay, the *rrf-3(pk1426)* RNAi sensitive strain was used.

Analysis of the fluorescence intensity in whole worm

For whole-animal fluorescence image, day 2 adult worms were anesthetized with 50 mM sodium azide, and imaged using a Leica M165 FC dissecting microscope. To quantify fluorescent intensity, the entire intestine regions were outlined and quantified using

ImageJ software. For quantification of the DVE-1::GFP, number of intestine nuclei with strong GFP signal were scored referred to previous study (Zhu et al., 2020). Confocal images were taken using Zeiss LSM980.

Western Blot analysis

Age synchronized worms were grown on plates containing OP50 bacteria at 20°C. 30–150 day 1 adult worms were picked into 20 μL M9 buffer and frozen in liquid nitrogen. The samples were stored at −80°C until all of them are ready for analysis. Before running the Western blot, 5× SDS loading buffer were added to each sample, mixed well and boiled for 15 min and resolved by Bio-Rad gels. For Western blot in non-reducing conditions, mixed stage worms grown on plates containing OP50 bacteria at 20°C were collected and washed with M9 buffer. After washing, the worms were resuspended in 0.5 volumes of extraction buffer [50 mM tris-HCl (pH 7.4), 150 mM NaCl, 0.5% NP-40, and protease inhibitors]. The suspension was then added into liquid nitrogen and grinded using mortar and pestle. The homogenized worm tissue was resuspended with 2 volumes of extraction buffer and lysed at 4°C for 30 min. The samples were then lysed with 4× LDS sample buffer (Pierce, 84,788), with or without reducing agent (Thermo Scientific, NP0009). Samples were boiled or heated at 70°C for 5 min and run on an SDS-PAGE gel before blotting to a PVDF membrane. Membranes were probed with antibodies against RFP (Rockland, 600-401-379s) or GFP (Santa Cruz Biotechnology, sc-9996).

Antibodies

Antibodies used for Western blot analysis were as follows: anti-GFP antibody (Santa Cruz Biotechnology, sc-9996) (1:1000); anti-Tubulin antibody (Sigma, T6074) (1:10000); anti-RFP (Rockland, 600-401-379s) (1:1000), anti-mouse secondary antibody (EarthOx, E030110) (1:10000); anti-rabbit secondary antibody (EASYBIO, BE1010) (1:10000).

RNA isolation and quantitative PCR analyses

Total RNA was isolated using TRIzol (Invitrogen). Worms were synchronized and L4 or day 1 adult worms grown on NGM plates were washed off the plates using M9 buffer, and 1 mL TRIzol were added to the samples and homogenized by repeated freezing and thawing using liquid nitrogen. RNA was isolated according to manufacturer's instructions. DNA was wiped off using RQ1 RNase-Free DNase (Promega). cDNA was synthesized using the M-MLV Reverse Transcriptase (Invitrogen). Gene expression levels were determined by real-time PCR using iTaq Universal SYBR Green Supermix (Biorad) and Biorad CFX96 Real-Time PCR Detection Systems. Relative gene expression was normalized to act-1(T04C12.6) mRNA levels (Zhang et al., 2018b). In each experiment at least three biological samples were analyzed.

Lifespan analysis

Lifespan experiments were performed on NGM plates at 20°C as previously described (Dillin et al., 2002). For chronic oxidative or reductive stress assays, 5mM paraquat or 5mM DTT was added into NGM and young adult worms were transferred to paraquat- or DTT-containing NGM plates. To prevent progeny production, 100 μL of 10 mg/mL 5-fluoro-2′-deoxyuridine (FUdR) was added to seeded plates. Worms were synchronized by egg bleach and were grown on OP50 bacteria from hatch, and transferred to FUdR plates from L4 to early adulthood. Worms were scored every second day. All lifespan data are available in Extended Data Table S2. Prism6 software was used for statistical analysis. Log rank (Mantel-Cox) method was used to determine the significance difference.

Tunicamycin killing assay

Synchronized young adult worms of different genetic backgrounds were incubated in M9 containing 100 ng/μL tunicamycin for 20 h at 20°C, and recovered on a plate with seeded OP50 for 8 h before analyzing the survival rate.

CCCP killing assay

Synchronized young adult worms of different genetic backgrounds were incubated in M9 containing 200 μM CCCP for 3.5 h at 20°C, and recovered on a plate with seeded OP50 for 8 h before analyzing the survival rate.

QUANTIFICATION AND STATISTICAL ANALYSIS

All experiments were repeated at least three times with identical or similar results. Data represent biological replicates. Appropriate statistical tests were used for every figure. Data meets the assumptions of the statistical tests described for each figure. Statistical parameters, including the exact value of n and descriptive statistics (mean ± SEM) and statistical significance are reported in the Figures and the Figure Legends. Data are judged to be statistically significant when $p < 0.05$ by two-tailed Student's t test. In figures, asterisks denote statistical significance as calculated by Student's t test (*, $p < 0.05$, **, $p < 0.01$, ***, $p < 0.001$) as compared to appropriate controls.

Cell Reports, Volume *39*

Supplemental information

Protein disulfide isomerase PDI-6 regulates Wnt secretion to coordinate inter-tissue UPR^{mt} activation and lifespan extension in *C. elegans*

Xinyu Li, Jiasheng Li, Di Zhu, Ning Zhang, Xusheng Hao, Wenfeng Zhang, Qian Zhang, Yangli Liu, Xueying Wu, and Ye Tian

Figure S1

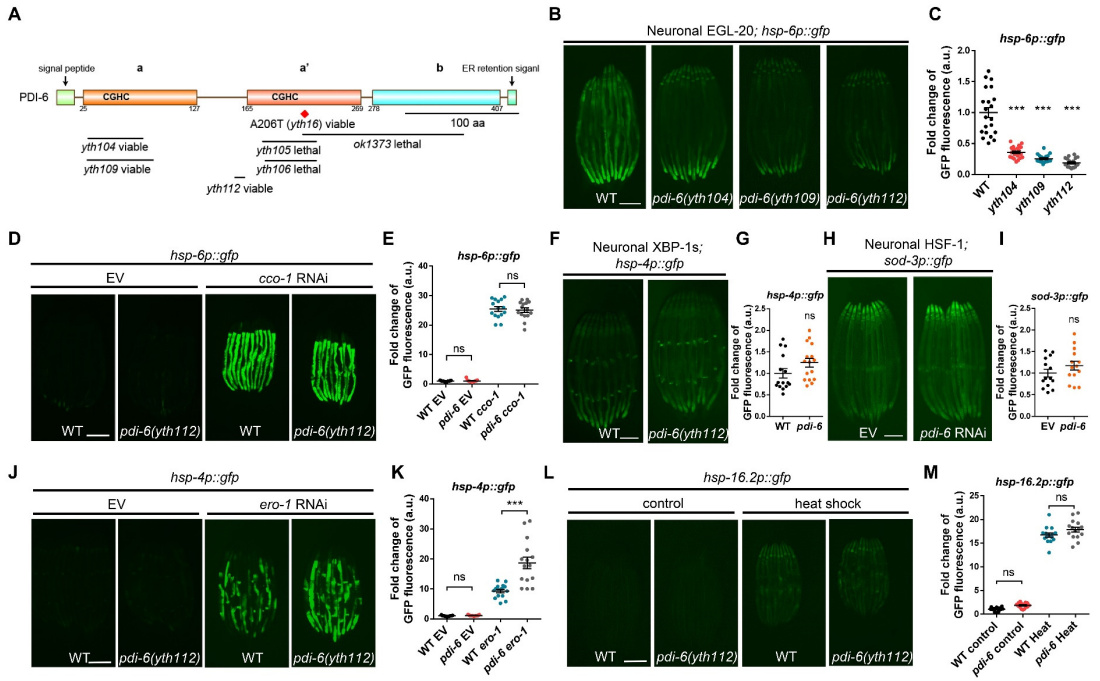

Figure S1. PDI-6 is not required for the induction of UPR^{ER} or UPR^{Cyt}. Related to Figure 1.

(A) Schematic representation of the protein domain structure and mutant alleles of *pdi-6* generated by CRISPR/Cas9-mediated gene editing. Scale bar = 100 amino acids (aa).

(B) Representative photomicrographs of day 1 adult animals expressing *rgef-1p::egl-20*; *hsp-6p::gfp* in WT and *pdi-6(yth104), pdi-6(yth109), pdi-6(yth112)* mutant animals.

(C) Quantification of *hsp-6p::gfp* expression as shown in (B).

(D) Representative photomicrographs of day 1 adult *hsp-6p::gfp* animals with the presence or absence of the *pdi-6* mutation grown on empty vector (EV) or with *cco-1* RNAi from hatching.

(E) Quantification of *hsp-6p::gfp* expression as shown in (D).

(F) Representative photomicrographs of day 1 adult animals expressing *rab-3p::xbp-1s* (*xbp-1* spliced form); *hsp-4p::gfp* in WT and *pdi-6* mutant animals.

(G) Quantification of *hsp-4p::gfp* expression as shown in (F).

(H) Representative photomicrographs of day 1 adult animals expressing *rab-3p::hsf-1*; *sod-3p::gfp* in WT and *pdi-6* mutant animals.

(I) Quantification of *sod-3p::gfp* expression as shown in (H).

(J) Representative photomicrographs of day 1 adult *hsp-4p::gfp* animals with the presence or absence of the *pdi-6* mutation grown on empty vector (EV) or with *ero-1* RNAi from hatching.

(K) Quantification of *hsp-4p::gfp* expression as shown in (J).

(L) Representative photomicrographs of day 1 adult *hsp-16.2p::gfp* animals with the presence or absence of the *pdi-6* mutation treated with heat shock (34 °C) or not.

(M) Quantification of *hsp-16.2p::gfp* expression as shown in (L).

***$p < 0.001$; ns = not significant ($p > 0.05$, t-test). Error bars = SEM; n ≥ 15 worms. Scale bar = 250 µm.

Figure S2

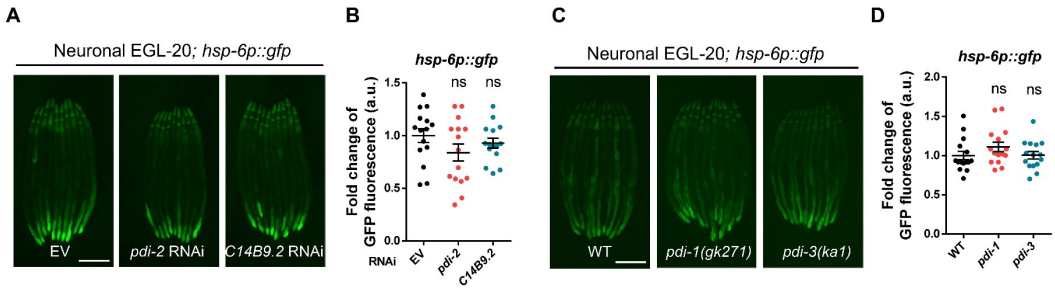

Figure S2. Other PDIs are not involved in the induction of cell non-autonomous UPR^{mt}. Related to Figure 2.

(A) Representative photomicrographs of day 1 adult animals expressing *rgef-1p::egl-20*; *hsp-6p::gfp* grown on empty vector (EV), *pdi-2* or *c14b9.2* RNAi bacteria from hatching. Scale bar = 250 µm.

(B) Quantifications of *hsp-6p::gfp* expression as shown in (A). ns = not significant ($p > 0.05$, t-test). Error bars = SEM; n ≥ 15 worms.

(C) Representative photomicrographs of day 1 adult animals expressing *rgef-1p::egl-20*; *hsp-6p::gfp* in WT, *pdi-1(gk271),* and *pdi-3(ka1)* mutant animals. Scale bar = 250 µm.

(D) Quantification of *hsp-6p::gfp* expression as shown in (C). ns = not significant ($p > 0.05$, t-test). Error bars = SEM; n ≥ 15 worms.

Figure S3

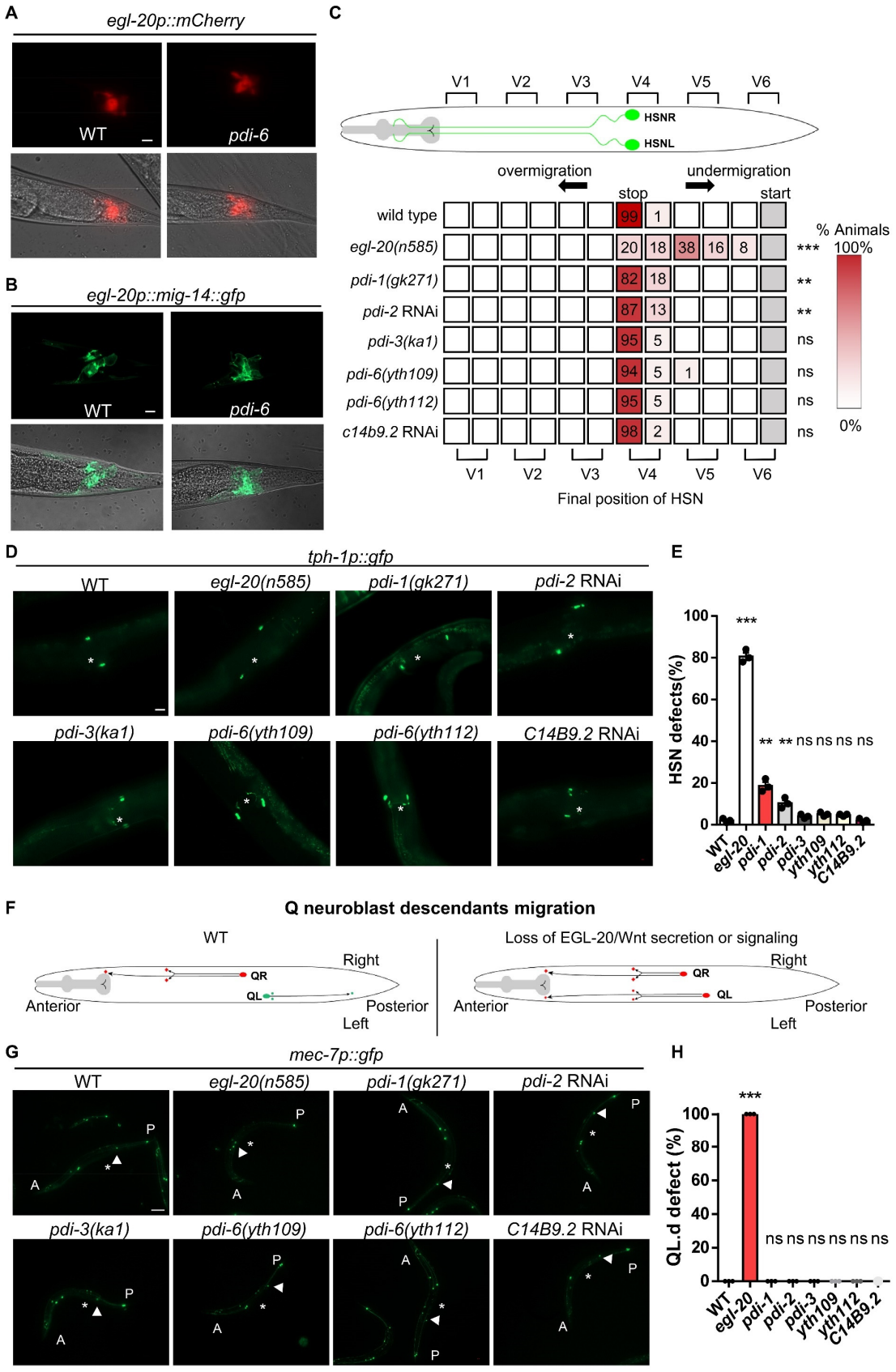

Figure S3. PDI-6 is not required for Wnt-directed hermaphrodite-specific neuron (HSN) or left Q neuroblast descendants (QL.ds) migration during early development. Related to Figure 3.

(A) Representative photomicrographs of day 1 adult animals expressing *egl-20p::mCherry* with the presence or absence of the *pdi-6* mutation. Scale bar = 10 μm.
(B) Representative photomicrographs of day 1 adult animals expressing *egl-20p::mig-14::gfp* with the presence or absence of the *pdi-6* mutation. Scale bar = 10 μm.
(C) Average position of the HSNs with respect to seam cells V1.a to V6.p in young adult WT, *egl-20(n585)*, *pdi-1(gk271), pdi-2* RNAi, *pdi-3(ka1)*, *pdi-6(yth109), pdi-6(yth112),* and *c14b9.2* RNAi animals (scored by Nomarski optics). Values listed are percentiles of the total number of cells scored; the red coded heatmap displays the range of percentile values.
(D) Representative photomicrographs of young adult animals expressing HSNs marker *tph-1p::gfp* in WT, *pdi-1(gk271)*, *pdi-2* RNAi, *pdi-3(ka1)*, *pdi-6(yth109)*, *pdi-6(yth112)*, *C14B9.2* RNAi. Asterisk indicates vulva position. Scale bar, 20 μm.
(E) Quantification of HSN migration defects as shown in (D).
(F) Schematic representation of Q neuroblast descendants (Q.ds) migration and the dependency of this migration on Wnt signaling. Dorsal view, anterior is shown to the left. Cells are in green or red when *mab-5* expression is activated or absent, respectively. In WT animals, the left Q neuroblast descendants (QL.ds) migrate to positions in the posterior part of the animal. In the absence of Wnt signaling, the QL.ds migrate in the opposite, anterior direction.
(G) Representative photomicrographs of young adult animals expressing *mec-7p::gfp* in WT, *pdi-1(gk271)*, *pdi-2* RNAi, *pdi-3(ka1)*, *pdi-6(yth109)*, *pdi-6(yth112)*, *c14b9.2* RNAi. Asterisk indicates vulva position; A indicates anterior side of the worm; and P indicates posterior part of the worm; white arrowhead indicates the QL.d. Scale bar, 100 μm.
(H) Quantification of QL.ds migration defects as indicated.
***$p < 0.001$, **$p < 0.01$, ns = not significant ($p > 0.05$, t-test). Error bars = SEM; $n \geq 3$.

Figure S4

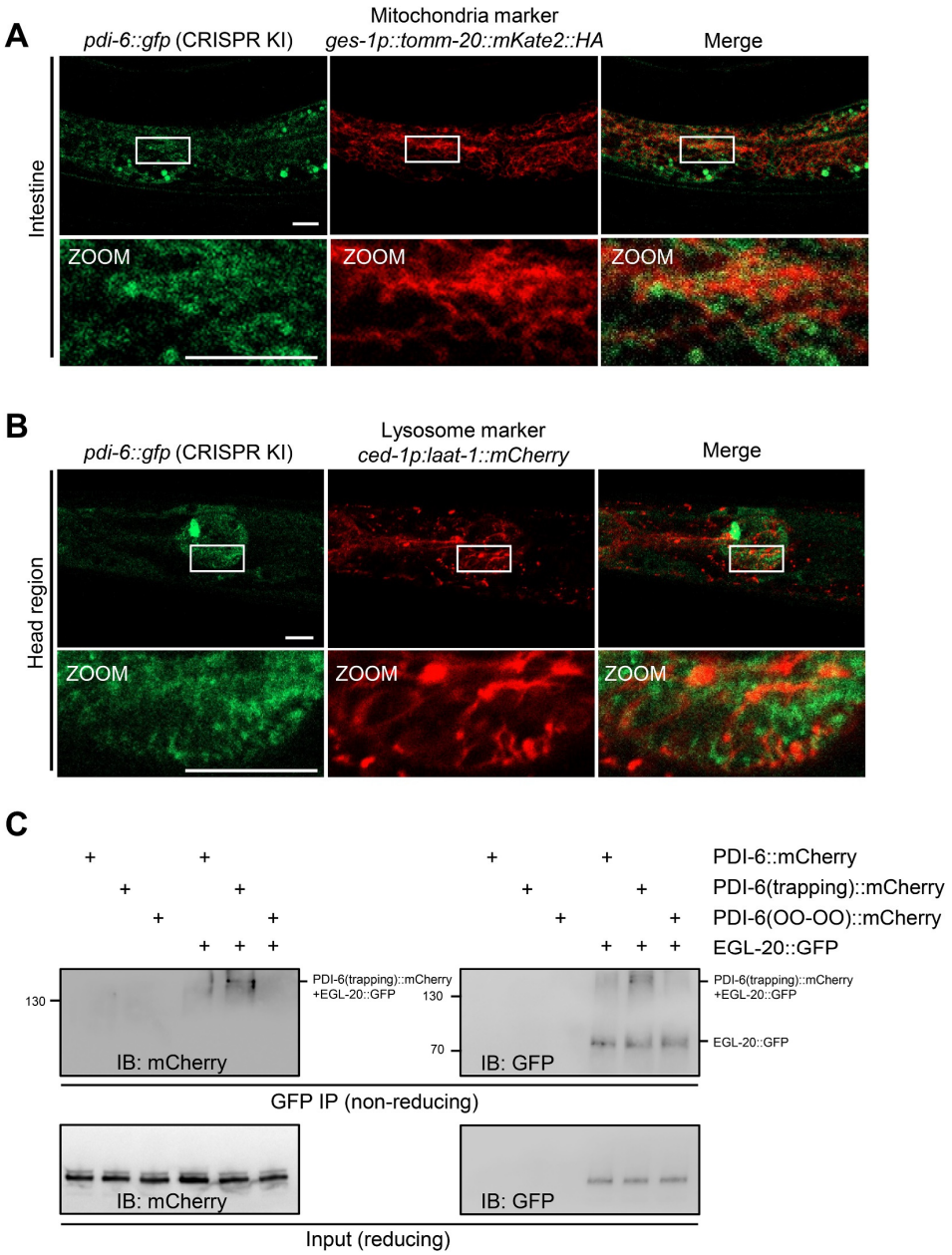

Figure S4. PDI-6 interacts with Wnt/EGL-20 potentially through intermolecular disulfide bonds. Related to Figure 4.

(A) Representative confocal photomicrographs of day 1 adult animals expressing *pdi-6::gfp* in combination with an intestinal mitochondrial outer membrane marker *ges-1p::tomm-20::mKate2::HA*. The panels below show high-magnification views of boxed regions. Scale bar = 10 μm.

(B) Representative confocal photomicrographs of day 1 adult animals expressing *pdi-6::gfp* in combination with a lysosomal membrane marker *ced-1p::laat-1::cherry*. The panels below show high-magnification views of boxed regions. Scale bar = 10 μm.

(C) Immunoblot of mCherry-tagged proteins (left) or GFP-tagged proteins (right) immunoprecipitated with the GFP-trap agarose from lysates of animals with overexpression of indicated proteins. The upper panels are of non-reducing and the lower panels are of reducing conditions.

Figure S5

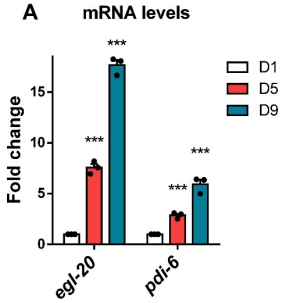

Figure S5. mRNA levels of *pdi-6* and *egl-20* increase with age. Related to Figure 5.

(A) Quantification of *egl-20* and *pdi-6* mRNA levels in day 1, day 5, and day 9 animals. $p < 0.001$ (t-test). Error bars = SEM; $n \geq 3$.

Figure S6

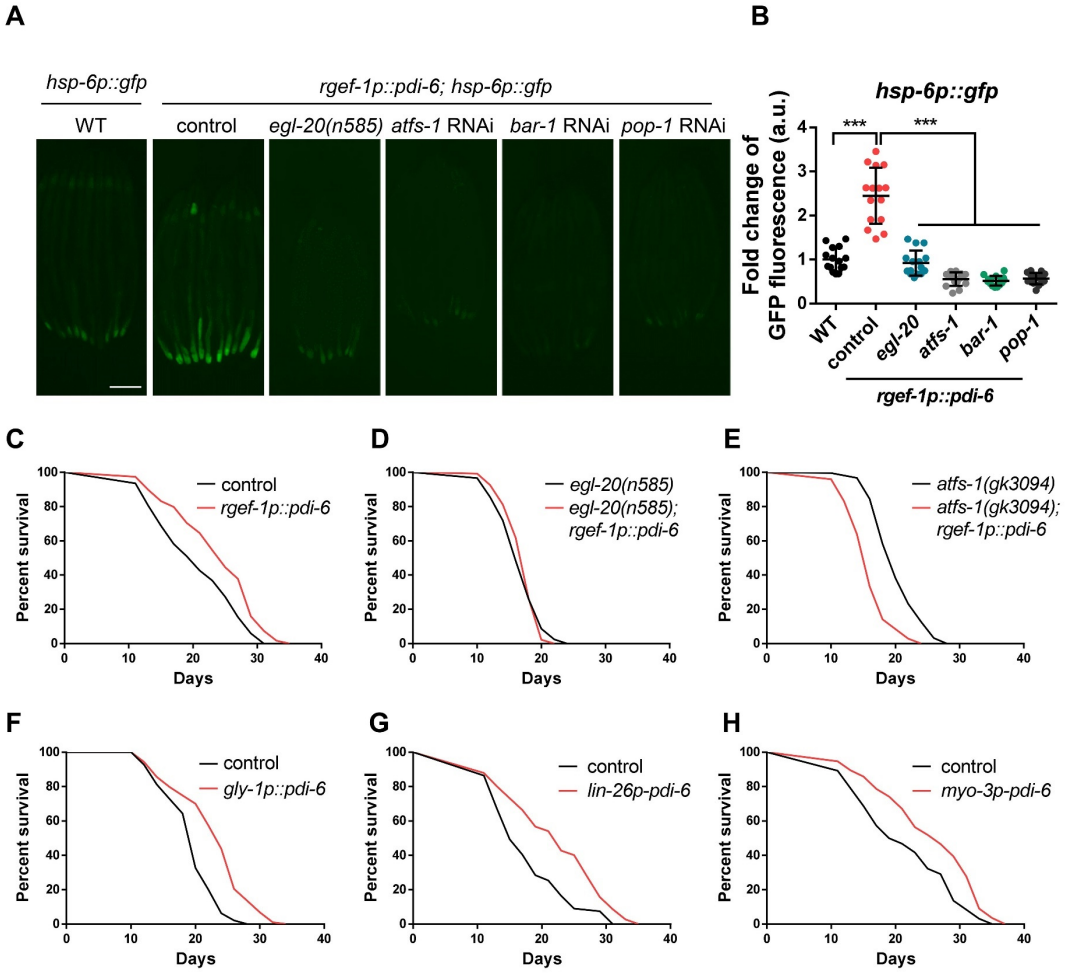

Figure S6. Overexpression of PDI-6 in neurons is sufficient to induce intestinal UPR^{mt} and extend lifespan in a Wnt/EGL-20-dependent manner. Related to Figure 6.

(A) Representative photomicrograph of day 1 adult animals expressing *hsp-6p::gfp* and *rgef-1p::pdi-6* in WT, *egl-20(n585)*, *atfs-1* RNAi, *bar-1* RNAi, and *pop-1* RNAi. Scale bar, 250 μm.

(B) Quantification of *hsp-6p::gfp* expression as shown in (A). $p < 0.001$ (t-test). Error bars = SEM; $n \geq 15$ worms.

(C) Survival analyses of control and *rgef-1p::pdi-6* overexpressing animals. $n \geq 100$ worms.

(D) Survival analyses of *egl-20(n585)* and *egl-20(n585)*; *rgef-1p::pdi-6* animals. $n \geq 100$ worms.

(E) Survival analyses of *atfs-1(gk3094)* and *atfs-1(gk3094)*; *rgef-1p::pdi-6* animals. $n \geq 100$ worms.

(F) Survival analyses of control and *gly-19p::pdi-6* expressing animals. $n \geq 100$ worms.

(G) Survival analyses of control and *lin-26p::pdi-6* overexpressing animals. $n \geq 100$ worms.

(H) Survival analyses of control and *myo-3p::pdi-6* overexpressing animals. $n \geq 100$ worms.

See Supplementary Table 1 for lifespan statistics.